1 Full Title: Meiotic DSB repair DNA synthesis tracts in *Arabidopsis thaliana*

2 Short Title: SPO11-dependent meiotic DNA synthesis.

3

4 Authors: Miguel Hernández Sánchez-Rebato[1&], Veit Schubert[2], Charles I. White[1]*

5

6 Affiliations:

7 [1] Institut de Génétique, Reproduction et Développement, CNRS UMR 6293, INSERM U1103,

8 Université Clermont Auvergne, 28, place Henri Dunant,

9 63001 Clermont-Ferrand, France.

10 [2] Leibniz Institute of Plant Genetics and Crop Plant Research (IPK) Gatersleben, D-06466

11 Seeland, Germany

12 [&]Current address: Centro de Biología Molecular Severo Ochoa,

13 Calle Nicolás Cabrera 1, 28049 Madrid, Spain

14

15 * Corresponding author.

16 E-mail: charles.white@cnrs.fr

17

18 Keywords: Meiosis, Recombination, DNA synthesis, DSB repair, SPO11

19

Abstract

We report here the successful labelling of meiotic prophase I DNA synthesis in the flowering plant, *Arabidopsis thaliana*. Incorporation of the thymidine analogue, EdU, enables visualisation of the footprints of recombinational repair of programmed meiotic DNA double-strand breaks (DSB), with ~400 discrete, SPO11-dependent, EdU-labelled chromosomal foci clearly visible at pachytene and later stages of meiosis. This number equates well with previous estimations of 200-300 DNA double-strand breaks per meiosis in Arabidopsis, confirming the power of this approach to detect the repair of most or all SPO11-dependent meiotic DSB repair recombination. The chromosomal distribution of these DNA-synthesis foci accords with that of early recombination markers and MLH1, which marks Class I crossover sites, colocalises with the EdU foci. Arabidopsis

It is currently estimated that ~10 cross-overs (CO) and an equivalent number of non-cross-overs (NCO) occur in each Arabidopsis male meiosis. Thus, at least 90% of meiotic recombination events, and very probably more, have not previously been accessible for analysis. Visual examination of the patterns of the foci on the synapsed pachytene chromosomes corresponds well with expectations from the different mechanisms of meiotic recombination and notably, no evidence for long Break-Induced Replication DNA synthesis tracts was found. Labelling of meiotic prophase I, SPO11-dependent DNA synthesis holds great promise for further understanding of the molecular mechanisms of meiotic recombination, at the heart of reproduction and evolution of eukaryotes.

Author Summary

Sexual reproduction involves the fusion of two cells, one from each parent. To maintain a stable chromosome complement across generations, these specialized reproductive cells must be produced through a specialized cell division called meiosis. Meiosis halves the chromosome complement of gametes and recombines the parental genetic contributions in each gamete, generating the genetic variation that drives evolution. The complex mechanisms of meiotic recombination have been intensely studied for many years and we now know that it involves the repair of programmed chromosomal breaks through recombination with intact template DNA sequences on another chromatid. At the molecular level, this is known to involve new DNA synthesis at the sites of repair/recombination and we report here the successful identification and characterisation of this DNA neo-synthesis during meiosis in the flowering plant, Arabidopsis. Both the characteristics and numbers of these DNA synthesis tracts accord with expectations from theory and earlier studies. Potentially applicable to studies in many organisms, this approach provides indelible footprints in the chromosomes and has the great advantage of freeing researchers from dependence on indirect methods involving detection of proteins involved in these dynamic processes.

61 ## Introduction

62 Meiosis is the specialised cell division that halves chromosome numbers during the
63 production of gametes, essential for the maintenance of stable ploidy across generations in
64 sexually-reproducing organisms. In contrast to mitosis, in which duplication of the genome is
65 followed by a single cellular division, meiosis involves one round of DNA replication followed
66 by two rounds of division. Separating sister chromatids to opposite poles, the second meiotic
67 division is, in broad terms, analogous to mitosis. Balanced chromosomal segregation during
68 the first division however requires that homologous chromosomes recognise each other, pair
69 and orient themselves on the spindle so that the two members of each pair move to opposite
70 poles during anaphase. This is ensured by the programmed induction of homologous
71 recombination through the induction and repair of DNA double-strand breaks (DSB) during
72 the first meiotic prophase.

73 This programmed, highly regulated process of DNA damage and repair is essential for
74 proper meiotic chromosome alignment and segregation and thus fertility in eukaryotes, with
75 some known exceptions, notably *Drosophila* and *C. elegans* (see review by [1]). Following the
76 programmed induction of DSB by the SPO11 complex, the cleaved DNA ends are resected to
77 produce 3'-ssDNA overhangs, onto which the recombinases DMC1 and RAD51 are loaded to
78 form presynaptic nucleoprotein filaments. These presynaptic nucleofilaments are the active
79 molecular species in the search for, and invasion of an intact homologous DNA template, the
80 first steps of DNA repair via homologous recombination. DNA synthesis then extends the
81 invading 3' end across the template and the joint-molecule intermediate structures are
82 further processed to yield the two main products of HR-mediated DSB repair: gene

83 conversions associated with reciprocal exchange of their flanking sequences (crossovers, CO),
84 or not (non-crossovers, NCO).

85 DNA synthesis is thus inherent to DSB repair via homologous recombination. In the
86 1960s, studies based on incorporation of H3-thymidine and C14-thymidine into newly
87 synthesised DNA gave evidence for meiotic prophase I DNA synthesis in the plants *Lilium*
88 *longiflorum* and *Trillium erectum*, the amphibian *Triturum viridescens*, mice and humans [2–
89 6]. These early studies have since been extended to show association of DNA synthesis with
90 pachytene recombination nodules in *Drosophila* female meiosis and with the synaptonemal
91 complex in mouse spermatocytes [7,8].

92 Labelling with 5-bromo-2′-deoxyuridine (BrdU) in budding yeast has been used to
93 confirm the presence of SPO11-dependent meiotic prophase DNA synthesis [9]. The authors
94 characterized both single-molecule BrdU tracts at a recombination hotspot and the timing of
95 their appearance in relation to other meiotic features. Observation of SPO11-dependent,
96 BrdU labelling pattern has also been described in *Tetrahymena* [10] but, to our knowledge,
97 no further data has been published in other organisms. In Arabidopsis, incorporation of BrdU
98 or 5-ethynyl-2'- deoxyuridine (EdU) during pre-meiotic S-phase has been used to establish
99 the meiotic timeline of meiosis in Arabidopsis pollen mother cells (PMC) [11–13]. There are
100 thus far no reports of labelling non-S-Phase DNA synthesis during Arabidopsis meiosis.

101 The induction of synchronous meiosis in populations of cells has been key to a number
102 of major advances in understanding of the molecular processes that make up the meiotic
103 division [14–18]. However, such direct approaches have not been available in other
104 organisms and this has resulted in significant gaps in understanding. A clear example of this is
105 seen in the flowering plant, *A. thaliana*. Estimations of numbers of SPO11-induced DSB in

106 Arabidopsis pollen mother cells (PMC, male meiosis) are ~200-300 per meiosis. Of these, ~10
107 yield inter-homologue CO and another 10 have been shown to give inter-homologue NCO
108 [19,20]. Thus, the repair outcome of at least 90% of meiotic DSB in Arabidopsis is not known.
109 The situation is strikingly different in budding yeast with 66 NCO plus 90.5 CO estimated per
110 meiosis, the sum of which is very close to the estimated 140-170 meiotic DSB. Similarly in
111 mouse, 273 NCO plus 27 CO sum close to the estimated 200-400 meiotic DSB [21–24].

112 Detection of recombination-associated DNA synthesis tracts offers an attractive path to
113 understand the mechanisms underlying these "invisible" meiotic recombination events in
114 Arabidopsis and potentially in other organisms. We present here the successful labelling of
115 SPO11-dependent, meiotic prophase I DNA synthesis by EdU incorporation in Arabidopsis
116 PMC.

117

118

119 Results

120 EdU labelling of DSB repair-associated DNA synthesis

121 In Arabidopsis, while each inflorescence contains flower buds bearing PMC at different
122 pre-meiotic and meiotic stages, the PMC of the anthers of a given flower bud are nearly
123 synchronous [25,26]. Along with the sequence of cytologically distinguishable meiotic stages
124 in the buds of a given inflorescence, in practice it is relatively straightforward to classify PMC
125 subpopulations within the meiotic timeline.

126 Timelines of Arabidopsis male meiosis concord that pre-meiotic G2 phase lasts 7-10
127 hours and that pollen mother cells advance from the beginning of leptotene to the end of

128 pachytene in 19 to 21 hours [11–13,27](summarized in Figure 1). Subsequent stages of
129 meiosis are considerably faster, with post-pachytene meiosis estimated to take from 2.7 to 9
130 hours. Given that meiotic DSB formation begins at the onset of prophase I (early leptotene)
131 and continues for a few hours [28], any meiotic prophase I DSB-repair DNA synthesis should
132 occur at least 7-10 hours after the end of pre-meiotic S-phase. We thus decided to incubate
133 the inflorescences with the nucleoside analogue for a 24-hour pulse to entirely cover the
134 prophase I DSB repair-associated DNA synthesis window. Given the relative synchrony of
135 progression through meiosis of the PMC from a given flower bud, the easily identifiable
136 appearance of S-phase labelling and the possibility to easily situate subpopulations of meiotic
137 cells in the temporal meiotic sequence, it seemed reasonable to expect that we would be
138 able to exclude S-phase labelled meioses, and thus focus our analyses on those labelled
139 during Prophase I.

140 Notwithstanding the current absence of direct evidence of the timing of occurrence of
141 meiotic recombination intermediates in Arabidopsis, DAPI staining and immunolocalisation of
142 meiotic proteins implicated in early invasion intermediates (RAD51/DMC1), joint molecules
143 (MSH4, early HEI10) and resolution (MLH1, late HEI10) give a clear picture of the progression
144 of key events through meiotic prophase I. In pachytene, when synapsis is complete, mean
145 numbers of MLH1 foci correspond to the number of Class I crossovers (~90% of total CO),
146 measured by counting of chiasmata at metaphase I. In analogy to organisms for which
147 recombination intermediates can be tracked directly, it is reasonable to assume that most
148 recombination events are either resolved or close to resolution at pachytene in Arabidopsis.

149 As summarised in Figure 1 , inflorescences were thus incubated with EdU for 24 hours to
150 ensure coverage of the window of DSB repair-associated DNA synthesis through prophase I

151 up to the end of pachytene. Pachytene cells observed at the end of the 24-hour pulse would
152 have traversed prophase I up to that point in the presence of the analogue. As mentioned
153 above, nuclei with pre-meiotic S-phase labelling were easily identified and excluded from the
154 analysis.

155

156 **Non-replicative DNA synthesis tracts are present from pachytene until the end of meiosis**

157 Early prophase I meiocytes, including cells in leptotene and zygotene, showed complete
158 or extensive EdU labelling of their chromosomes (Figure 2a). This replicative labelling
159 confirms, as expected, that they had passed through pre-meiotic S-Phase during the EdU
160 pulse [11–13,29,30]. Furthermore, nuclei with partial replicative labelling of DAPI-dense, late
161 replicating heterochromatic regions were observed, as expected for cells that were in
162 mid/late S-phase at the beginning of the EdU pulse (second row of Figure 2a) [30–33].

163 In striking contrast, pachytene nuclei showed faint, discrete foci of a considerably
164 smaller size (Figure 2a Pachytene, see also Figure 4a and Figure S1). These foci are very faint
165 through the microscope eyepiece, but are clearly visible when the images are processed. This
166 difference in labelling intensity between S-phase and prophase EdU incorporation is not
167 unexpected, considering that the latter would correspond to DNA synthesis tracts of tens to a
168 few thousands of base pairs, while replicative DNA synthesis would range from megabase-
169 long late-replicating regions to the whole genome (4C ≈ 520 Mb in these prophase I nuclei)
170 [34]. We note also the presence of labelled mitochondria in these images, confirming their
171 replication during pre-meiotic G2 and/or meiotic prophase I cells. These labelled
172 mitochondria, clearly visible from pachytene on, are also present at earlier stages, but are not

173 readily visible due to the very strong fluorescence of the S-phase replicative nuclear labelling
174 (Figure 2).

175 The EdU foci observed in pachytene cells appear well-distributed across the
176 chromosomes, but are less present in DAPI-dense, heterochromatic regions (Figure 2a
177 Pachytene, Figure 4a). Furthermore, given the tighter-packed DNA in these regions, the
178 observed lesser density of EdU foci is presumably an underestimation. This pattern of foci
179 concords with genetic crossover mapping, studies of meiotic DSB (SPO11-oligo sequencing)
180 and immunofluorescence studies of the distributions of early recombination proteins, all of
181 which show meiotic recombination to follow a relatively even distribution across the
182 Arabidopsis genome, with the exception of (heterochromatic) centromeric regions which
183 have significantly lower densities of SPO11-oligos and crossovers [34–36].

184 As summarised in Figure 1, based on published timelines [11–13,27] and our own
185 measurements, a meiocyte observed at the telophase II/tetrad stage would have been at
186 leptotene/zygotene at the beginning of the 24-hour EdU pulse. We had thus good reason to
187 expect that prophase I EdU foci would be observable in all meiotic stages up to the end of
188 meiosis. This was indeed the case, with EdU foci visible from pachytene to the end of meiosis
189 (telophase II/tetrad Figure 2). Meiotic chromosomes condense progressively as they traverse
190 prophase I, evolving from a mass of hardly-distinguishable thin fibres at early leptotene to
191 thick synapsed fibres in pachytene and to individualised dense bivalents with a more
192 polygonal shape at metaphase I. This condensation produces significant shortening of the
193 chromosomes and results in changes of the visual character of the EdU signals. While most
194 EdU foci at pachytene appear as discrete spots, they merge into larger patches at diplotene
195 and this continues through diakinesis, up to the greatest condensation at metaphase I (Figure

196 2, diplotene-metaphase I). Furthermore, heterochromatic, centromeric regions become
197 more easily identifiable when bivalents individualize at diakinesis and the relatively low
198 density of EdU signals in these regions becomes clearly visible. This is even more pronounced
199 at metaphase I, with clear visual differentiation between the centromeric and
200 pericentromeric regions of the two homologous chromosomes of each bivalent. Finally, the
201 EdU signals are observed throughout the second meiotic division, changing their appearance
202 with evolving chromosome condensation and shape in a way similar to that seen during the
203 first meiotic division (Figure 2, prophase II-tetrad).

204

205 Prophase I DNA synthesis is SPO11-dependent

206 Meiotic recombination is initiated by the induction of DNA DSB by the SPO11 complex at
207 the beginning of meiotic prophase I. To verify that the discrete non-replicative DNA synthesis
208 tracts observed at pachytene and subsequent stages originate from SPO11-dependent
209 meiotic DSB repair, we carried out this analysis in parallel in *spo11-1* mutant plants [37]
210 (Figure 3). Pachytene images were analysed with the IMARIS software package (Bitplane AG,
211 Oxford Instruments, UK) *Spots* function. EdU foci were selected based on diameter and mean
212 intensity in the EdU channel, and filtered to retain only those colocalising with chromosome
213 fibres (mean intensity cutoff in the DAPI channel). A high-cut filter of mean intensity in the
214 EdU channel was also applied to filter out the much-brighter organellar foci.

215 WT pachytenes show 409.5 ± 7.96 EdU foci per nucleus (mean ± SEM; n = 45 nuclei;
216 Figure 2, Figure S1), with counts ranging from 323 to 510 (plus one outlier with 263). Ten of
217 the 45 image stacks analysed were acquired via 3D-SIM, for comparison with the Zeiss LSM
218 800/Airyscan confocal image stacks and to confirm that we were not missing foci. WT cells

219 imaged with 3D-SIM had a mean 400.6 ± 14.74 EdU foci (n = 10) while those imaged with the
220 confocal microscope had a mean of 412.1 ± 9.38 EdU foci (n = 35). Hence, no significant
221 difference was observed between both imaging systems (unpaired t-test; p = 0.55) (Figure 4).

222 In *spo11-1* plants, 39.2 ± 2.83 EdU foci per cell (mean ± SEM; n = 35 cells; Figures 3, 4)
223 were detected in zygotene/pachytene nuclei. Thus, some EdU foci were detected in *spo11-1*
224 meioses, but in significantly lower numbers and, in general, considerably smaller and weaker
225 than the foci in the WT. A similar signature could be observed in *spo11-1* cells at subsequent
226 meiotic stages (Figure 3, diakinesis to Telophase II), with some EdU foci detected but in much
227 lower numbers. This ~10-fold reduction in mean numbers of foci with respect to the WT is
228 highly significant (unpaired t-test; p < 0.0001) and confirms the SPO11-dependence of the
229 great majority of the observed pachytene EdU foci. That the expected S-phase EdU labelling
230 was observed in early prophase I *spo11-1* PMC nuclei (Figure 3, early PI, mid PI, second row)
231 and organellar EdU labelling was comparable in *spo11-1* and WT meioses (Figures 2, 3),
232 confirms that the EdU labelling pulse worked as expected in both WT and *spo11-1* plants.

233 In interpreting these numbers it is important to note that although Arabidopsis *spo11*
234 meiosis does complete and produce (mostly inviable) pollen, chromosome pairing and
235 synapsis are very severely reduced in *spo11* meiosis and the zygotene/pachytene stages are
236 only identifiable by their characteristic chromosome condensation and their temporal
237 positioning [37]. Thus, *spo11-1* PMC at leptotene can be differentiated from the zygotene-
238 like state by the condensation of the chromosomes (thickness of the fibres) and the
239 clustering of DAPI-dense regions. Also, *spo11-1* zygotene/pachytene-like cells that do not
240 show S-phase EdU labelling are in a more advanced state that those that do show it, as they
241 would have completed S-phase at the beginning of the pulse (Figure 3a, mid PI, third row vs

242 second row). Identification of later meiotic stages in *spo11-1* meioses presents no difficulties
243 (Figure 3).
244

245 Prophase I DNA synthesis patterns mirror meiotic recombination features

246 Meiotic recombination models predict different patterns of DNA synthesis tracts
247 depending on how recombination intermediates are formed and resolved. Non-crossover
248 events generated by either synthesis-dependent strand annealing (SDSA) or dHJ dissolution
249 recombination, both expected to produce DNA synthesis tracts in only one of the two
250 implicated chromatids and thus in only one of the homologous chromosomes in
251 interhomologue recombination. On the other hand, dHJ resolution resulting in either
252 crossover or non-crossover products would generate DNA synthesis tracts in both
253 participating chromatids - and both chromosomes in interhomologue events.

254 The expected patterns of resulting EdU foci are shown schematically in Figure 5a and
255 examples of segments of the synaptonemal complex (SC) from SIM pachytene micrographs
256 are shown in Figure 5b. The paired, homologous chromosomes are clearly distinguishable in
257 these images, permitting a first analysis of different patterns of EdU foci. No obvious bias is
258 visible in the disposition of Individual EdU foci in these images. Foci are seen at both the
259 internal (facing the homologous chromosome) and external faces of the paired chromosomes
260 in the SC fibre, as well as in the middle of the SC (Figure 5).

261 Differences can however be seen when EdU foci are analysed with respect to adjacent
262 foci, with three clear configurations of pairs of foci, examples of which are circled on the
263 images shown in Figure 5b:

264 Class (1) isolated individual foci located on one of the two homologues (one SC lateral
265 axis; Fig. 5b, white circle).

266 Class (2) "pairs" of foci on one of the two homologues (one SC lateral axis; Fig. 5b,
267 green circle).

268 Class (3) "pairs" of foci on the two homologues (both SC lateral axes; Fig. 5b, yellow
269 circle).

270 Further examples of these patterns can be found in the pachytene images of Figure S2.

271 Finally, we note the absence of the long labelling tracts expected from BIR
272 recombination, implying that such events are either rare or "short", or both, in Arabidopsis
273 meiosis.

274

275 Prophase I DNA synthesis colocalize with class I crossovers

276 As the SPO11-dependent, meiotic prophase I DNA synthesis foci result from
277 recombinational repair of meiotic DSB, genetic crossovers should co-localize with a subset of
278 these EdU foci. Class I CO are detectable cytologically in Arabidopsis by the immunolocalization
279 of proteins such as MLH1.

280 Combining labelling of EdU tracts with immunolocalization of MLH1 (Figure 6) gave 7.86
281 ± 0.24 (mean ± SEM; n = 29) MLH1 foci per WT pachytene, as expected [38]. 95.6% (n=228) of
282 all MLH1 foci colocalized with an EdU focus and the remaining 4.4% were adjacent to one.
283 Although this conclusion must be tempered due to the high number of EdU foci in these
284 images, Arabidopsis Class I CO are thus physically associated with the prophase I DNA synthesis
285 tracts at this level of resolution.

286

287 # Discussion

288 ## Identification of meiotic DNA repair-associated DNA synthesis tracts

289 We present here the labelling and characterisation of SPO11-dependent, meiotic
290 prophase I DNA synthesis tracts through incorporation of the thymidine analogue EdU in
291 pollen mother cells of Arabidopsis plants. By labelling DNA synthesis associated with the
292 repair of meiotic DSB, this approach holds great promise for the future understanding of
293 recombination patterns and mechanisms, notably for studies of NCO and sister-chromatid
294 exchange (SCE) recombination. For practical reasons, molecular and genetic studies of
295 meiotic recombination have essentially been focussed on events implicating the transfer of
296 DNA sequence polymorphisms between the two recombining DNA molecules. The necessary
297 presence of such polymorphism has, for instance, complicated significantly the analysis of the
298 roles of meiotic SCE [39–46] and while EdU labelling has recently been applied to analysis of
299 meiotic sister-chromatid CO in *C. elegans* (Almanzar *et al*, 2021; Toraason *et al*, 2021;
300 Billmyre & Hughes, 2021), this approach does not appear adapted to the study of NCO.

301 Detection of NCO events in Arabidopsis has been elusive. Mapping NCO genome-wide by
302 sequencing Arabidopsis tetrads has estimated NCO numbers to be of the same order as CO,
303 ~10 events per meiosis, with gene conversion tracts ranging between a few tens to a few
304 hundreds of bp [19,20,50,51]. Notwithstanding this (surprisingly) low number of NCO,
305 numbers of CO are in agreement with chiasmata counting and immunolocalisation of CO
306 markers. Thus, given the 200-300 DSB per meiosis in the these cells, the repair of at least 90%
307 (and very possibly >98% [52] of meiotic DSB in Arabidopsis is not accessible to analysis with

308 current methods. In this work, we present the development of meiotic prophase DNA
309 synthesis labelling as a means to fully characterise meiotic DSB-repair in Arabidopsis
310 meiocytes.

311 Initial tests showed that incubating inflorescence stems for 24 hours in EdU solution
312 resulted in two clear sub-populations of meiocytes, distinguishable by their meiotic stage and
313 pattern of EdU labelling. The first consists of late G2 + early prophase I cells (leptotene,
314 zygotene) whose chromosomes show very strong EdU signals, either genome-wide or in large
315 patches. These patterns are consistent with those expected from pre-meiotic S-phase
316 replicative EdU incorporation:

317 I) This extensive EdU labelling is observed in meioses of both wild-type and *spo11* mutant
318 plants.

319 II) The extensive and intense fluorescent signals are similar to those observed in previous
320 reports of EdU/BrdU incorporation during pre-meiotic replication [11–13,29].

321 III) Extrapolating from published meiotic timelines and our own studies, PMC in pre-
322 meiotic S-phase at the beginning of the pulse are expected to advance at most to
323 leptotene-zygotene during the 24 hour EdU pulse (see Figure 1).

324 IV) The signal in partially labelled early prophase I cells corresponds principally to late-
325 replicating, DAPI-dense, heterochromatic regions, in accordance to expectations for cells
326 in late S-phase at the beginning of the EdU pulse.

327 The second population of EdU-labelled meiocytes includes cells at meiotic stages from
328 pachytene to the end of meiosis (tetrads), whose chromosomes show much fainter, discrete
329 EdU labelling. Clearly resolving into individual foci at the stages in which the chromosomes
330 are less condensed, these foci group into "patches" as chromosome condensation proceeds

331 post-prophase I. These foci have a number of characteristics which permit their identification
332 with confidence as meiotic DSB repair-associated DNA synthesis tracts:

333 I) These discrete EdU-label foci are SPO11-dependent, analogously to earlier
334 observations in yeast [9], confirming with high confidence that they result from EdU
335 incorporation at DNA synthesis tracts associated to meiotic DSB repair. Some EdU foci are
336 observed in *spo11-1* meioses, although at considerably lower numbers than in the wild type
337 (39 versus 410 per meiosis respectively). While some of these may come from mistaken
338 assignation of organellar DNA foci, we note that some crossing-over is detected in
339 Arabidopsis *spo11* plants, RAD51 foci are detected in Arabidopsis *spo11* meiosis and DMC1
340 foci in rice meioses [37,53–55]. Furthermore, given that both meiotic Arabidopsis SPO11
341 proteins are needed for normal meiotic DSB induction, some leakage may occur in plants
342 lacking one or the two SPO11 proteins [54,56–59]. Alternatively, they may correspond to
343 SPO11-independent breakage of mechanical, chemical or enzymatic origin. If so, that they do
344 produce DNA neo-synthesis tracts argues for their repair by HR rather than End Joining.

345 II) The SPO11-dependent foci are seen at later meiotic stages than those with replicative
346 labelling and these nuclei had thus completed S-phase prior to the beginning of the pulse.
347 Given the known timing of meiosis in these cells, meiotic DSB repair DNA synthesis will have
348 occurred during the EdU pulse in these cells [9,13,14,38,60]. We note that while present in
349 considerably lower numbers than in the wild type (39 versus 410 per meiosis, respectively),
350 there are some EdU foci in *spo11-1* meioses.

351 III) The discrete EdU foci observed at pachytene and later stages are both much less
352 intense and smaller in size than the generalised labelling in leptotene-zygotene nuclei. This is
353 expected given the predicted size of DNA synthesis tracts associated to recombination events

354 (few bases to some kilobases of DNA), with respect to replicative labelling (megabases to the
355 full genome).

356 IV) The numbers of EdU foci measured at pachytene concord with published estimations
357 of numbers of meiotic DSB and HR intermediates in Arabidopsis. A mean of 409.5 ± 7.96
358 (mean ± SEM; n = 45 meioses) DNA repair-associated DNA synthesis foci were observed in
359 WT pachytenes. This number is a little higher than estimations of meiotic DSB numbers
360 through immunolocalisation of early recombination proteins in Arabidopsis (RAD51 in most
361 cases). Reported numbers of RAD51 foci per Arabidopsis meiosis range from 90 to 250 per
362 meiosis, and compare well with a recent report of 239 ± 30 (mean ± SD) prophase I SPO11-1
363 foci [56]. Given the limitations of immunodetection and that the recruitment/release of these
364 proteins at DSB/recombination sites is dynamic, these numbers presumably under-estimate
365 the true values. Notably, a recent report using a STED super-resolution microscope found
366 more than 1000 RAD51 foci per PMC meiosis [52]. Thus, the mean of 409.5 DNA repair-
367 associated synthesis tracts per meiosis reported here is probably closer to the true value than
368 that of protein-immunodetection approaches. It is of course necessary to take into account
369 the fact that resolution of dHJ recombination intermediates is expected to result in patches
370 of neo-synthesized DNA on both implicated chromatids, resulting in two foci from a single
371 recombination event. Such events are however estimated to represent ~5% or less of meiotic
372 DSB repair events in Arabidopsis and so are not expected to impact significantly the
373 estimations of total events.

374 V) DAPI-dense heterochromatic, centromeric regions have a visibly lower density of
375 SPO11-dependent EdU foci in pachytene/diplotene and beyond (particularly noticeable at
376 diakinesis/MI). This concords with SPO11-oligo mapping of meiotic DSB patterns in

377 Arabidopsis PMC, which shows that centromeric regions have a much lower density of DSB
378 than the rest of the chromosome [34,36] .

379 VI) Combining labelling of EdU tracts with immunolocalization of MLH1 confirms that, as
380 expected, Class I CO are physically associated with the prophase I DSB repair DNA synthesis
381 tracts (Figure 6).

382

383 **Meiotic DSB repair-associated DNA synthesis tracts mirror meiotic recombination**
384 **features**

385 As presented in Figure 7, different mechanisms of recombinational repair of meiotic DSB
386 will result in different patterns of DNA synthesis tracts associated to an HR event. The most
387 obvious difference is that DNA synthesis is expected to be found on only the recipient
388 chromatid, which carried the initiating DSB (Figure 7f), or on both the recipient and donor
389 chromatids (Figure 7g, h). SDSA and dHJ dissolution mechanisms would lead to the former
390 and dHJ resolution to the latter. A special case is the BIR mechanism, which is expected to
391 result in a long DNA synthesis tract, potentially extending all the way to the end of the
392 recipient chromatid (Figure 7c).

393 Visual inspection of the pachytene images clearly shows different configurations of the
394 EdU foci, which we have arbitrarily divided into 3 classes suggestive of the DNA synthesis
395 patterns expected at sites of recombination:

396 Class (1) isolated individual foci located on one of the two homologues (one lateral axis)
397 (Fig. 5b, Fig. S2). Only the initially broken chromatid (recipient) will bear (EdU-substituted)

398 neosynthesized DNA tracts in repair via SDSA (Fig. 7a, b, f) and dHJ dissolution (Fig. 7a, d, e, f)
399 recombination.

400 Resolution of double Holiday junction (dHJ) intermediates (Fig7d) can give rise to gene
401 conversions, accompanied (Fig. 7g) or not (Fig. 7h) by a CO. In both cases, this can lead to the
402 presence of neo-synthesized DNA on both the donor and recipient chromatids. These events
403 would thus be expected to result in paired DNA synthesis tracts on the two participating
404 chromatids: either on one chromosome (Class (2) - one lateral axis) for sister chromatid
405 events, or on both homologues (Class (3) - both lateral axes).

406 Class (2) are thus "pairs" of foci on one of the two homologues (one SC lateral axis),
407 which could result from recombination between sister chromatids through the dHJ resolution
408 pathway.

409 Class (3) are "pairs" of foci on the two homologues (both lateral axes), which could result
410 from recombination between homologues through the dHJ resolution pathway.

411

412 We find no evidence for long DNA synthesis tracts indicative of BIR recombination in our
413 images. Thus, either BIR replication tracts are not distinguishably longer than other DSB
414 repair-DNA synthesis, or the BIR mechanism is a minor (or non-) contributor to DSB repair in
415 Arabidopsis meiosis. In this context, we note that an earlier effort to detect mitotic BIR repair
416 in bleomycin-treated *Vicia faba* root tips described asymetric interstitial G2-phase EdU
417 labelling of interstitial tandem-repeat regions, although no extended labelling tracts out to
418 the end of the chromatid were observed [61].

419

420 Inference of the recombination pathways underlying the 3 classes of foci of course
421 remains speculative in the absence of molecular analyses of the EdU tracts themselves. FISH
422 on extended DNA fibres was used in an earlier study in yeast to determine the lengths and
423 positioning of BrdU-substituted DNA synthesis tracts with respect to DSB hotspots [9]. They
424 observed two main classes of tracts: tracts that extended from the DSB towards only one side
425 of the DSB and tracts that extended on both sides. These two classes correspond to the tracts
426 expected in single DNA molecules that took part in CO events in the first case and NCO
427 events via SDSA in the second, which were further validated studying their dynamics in
428 recombination mutants. We have previously carried out DNA combing plus fibre FISH in
429 Arabidopsis [62], but the lack of strong meiotic DSB hotspots with a precisely localised DSB
430 site complicates the possible use of this approach in Arabidopsis meiosis. Rather, we are
431 actively developing an approach based on the direct detection of EdU-substituted DNA tracts
432 by Nanopore sequencing. It is hoped that this approach will permit unambiguous
433 characterisation of the principal meiotic recombination products and underlying mechanisms
434 in Arabidopsis, as well as of more complex events.

435

436

437

438

439 ## Materials and Methods

440 ### Plant material and growing conditions

441 Standard conditions were used for growth of wild-type *A. thaliana Col-0* and *spo11*-1-2
442 [37] plants. Seeds were sown on soil substrate (Klasmann-Deilmann GmbH TS3 FIN 416GF,
443 Geeste, Germany), stratified for 2-4 days at 4°C and grown in climate chambers at 23°C and
444 60% relative humidity, under a daily cycle of 16 hours of light (110-140 µmol m^{-2} s^{-1}) and 8
445 hours of darkness.

446 ### Meiotic chromosome preparation by spreading

447 Meiosis was analysed following the chromosome spreading method of Ross et al. [63],
448 with minor modifications. Inflorescences were collected in 3:1 ethanol:glacial acetic acid
449 fixative solution and left overnight at room temperature. The fixative was then substituted
450 with fresh fixative solution and the tubes were transferred to 4°C. This step was repeated the
451 following 2-3 days. At this point, fixed inflorescences can be stored at 4°C for further use or
452 prepared for microscopy.

453 A number of fixed inflorescences were selected, deposited in a glass dissection well with
454 3:1 fixative solution and dissected under a stereomicroscope into individual flower buds,
455 discarding open flowers and buds with pollen (yellow anthers). The flower buds were then
456 washed 3 x 2 minutes in citrate buffer and the buffer replaced with 500 µl of digestion
457 enzyme mix (0.3% w/v cellulase from *Trichoderma* sp. (Sigma-Aldrich), 0.3% w/v pectolyase
458 from *Aspergillus japonicus* (Sigma) and 0.3% w/v cytohelicase from *Helix pomatia* (Duchefa
459 Biochemie) in citrate buffer). The flower buds were incubated in the digestion mix for 2 hours
460 at 37°C and the digestion stopped by adding a greater volume of ice-cold citrate buffer. The

461 well was placed under the stereomicroscope and a single flower bud with a small volume of
462 liquid was transferred to a slide with a Pasteur pipette. The flower bud was macerated with a
463 needle, a 10µl drop of ice-cold 60% glacial acetic acid was added and the slide incubated for
464 one minute on a hot plate at 45°C while gently moving the drop with a flat needle. After the
465 incubation, an extra 10 µl of ice-cold 60% glacial acetic acid were added, followed by 100 µl
466 of 3:1 fixative - first circling and flooding the drop and then mixing with the drop by
467 vigorously pipetting the last microliters. The liquid was drained by tilting the slide, which was
468 then further washed with another 100 µl of 3:1 fixative, drained and left to air dry at room
469 temperature.

470 To visualize the chromosomes, the slides were stained in Vectashield antifade mounting
471 medium with 1.5 µg/ml DAPI (# H-1200, Vector Laboratories, Burlingame, CA, USA), by
472 putting a drop on a coverslip which was then placed on a slide and gently squashed by thumb
473 pressure. Spreads were analysed with a Zeiss AxioImager Z1 microscope with a 100×/1.40 Oil
474 Plan-Apochromat objective and the Zeiss ZEN2Blue software (Carl Zeiss GmbH)in the channel
475 for blue fluorescence (Zeiss #49 HE filter).

476 EdU labelling and cytological detection

477 Among the different thymidine analogues commonly used to label *in vivo* DNA synthesis,
478 5-Ethynyl-2'-deoxyuridine (EdU) has a number of advantages and has been preferred by the
479 Arabidopsis community in recent studies labelling DNA synthesis [12,29,30,64–67]. EdU can
480 be detected in intact double-strand DNA and this antibody-free technique simplifies the
481 protocol and offers better reproducibility.

482 EdU (#Ab146186, Abcam, UK) working solutions were prepared at 10mM in 1×PBS
483 buffer. Arabidopsis stems with apical inflorescences were submerged in water to avoid the

484 introduction of air bubbles (submerging only the stem segment to be cut, without wetting
485 the inflorescences) and cut obliquely 4-5cm below the inflorescence. Care was taken to make
486 the cleanest cut possible in order to avoid crushing vascular tissues. Open flowers and big
487 leaves (if present) were removed to avoid crowding the tube and minimize the risk of
488 exhausting the solution due to excessive transpiration. The inflorescences were incubated in
489 800µl of 10mM EdU in a 2ml eppendorf tube for 24 hours, under the same growing
490 conditions as the plants. To avoid tight packing, a maximum of four or five inflorescence
491 stems were incubated in one tube. After 24 hours the inflorescences were removed from the
492 EdU solution and fixed in 3:1 ethanol:glacial acetic acid solution.

493 Chromosome spreads were prepared as previously described and visualised under the
494 microscope to identify those slides with meiocytes at the desired meiotic stages. The slides
495 were first incubated in 4T (4×SSC, 0.5% v/v Tween 20) in a Coplin jar until the coverslips
496 detached, followed by 30' without coverslips in fresh 4T. The Click-iT reaction mix (Invitrogen
497 Click-iT plus Alexa-fluor 647 kit, Thermo-Fisher Scientific) to label EdU with the fluorochrome
498 was prepared following the manufacturer's instructions. Before labelling, the slides were
499 washed for 5 minutes with 1×PBS. A 30µl drop of Click-iT reagent was placed on a 32x24mm
500 piece of parafilm and the inverted slides were placed on top of the mix on the parafilm. The
501 slides were incubated with the mix for 30 minutes at 37°C in a dark moist chamber, washed
502 for 5 minutes with 1×PBS in a Coplin jar in the dark and mounted in Vectashield + DAPI for
503 microscopy.

504 Pictures were taken using a Zeiss LSM800 confocal microscope applying the Airyscan
505 module and selecting the presets for each specific dye. EdU foci were quantified semi-
506 automatically using the IMARIS software *Spots* tool (Bitplane AG, Oxford Instruments, UK),

507 adding intensity filters for both channels to specifically selected visually detectable EdU foci
508 that co-localised with the DAPI fluorescence of the chromosomes. To analyze the chromatin
509 and EdU signal ultrastructure, we applied super-resolution spatial structured illumination
510 microscopy (3D-SIM) using a 63×/1.40 Oil Plan-Apochromat objective of an Elyra PS.1
511 microscope system and the ZENBlack software (Carl Zeiss GmbH) [68]. Maximum intensity
512 projections were calculated from 3D-SIM image stacks. Zoom-in sections were presented as
513 single slices to indicate the subnuclear chromatin structures at the super-resolution level.

514 Detection of MLH1 and EdU

515 For the detection of MLH1 and neo-synthesized DNA tracts with incorporated EdU, the
516 protocol for the immunolocalization of MLH1 [69] was adapted to include the Click-iT EdU
517 labelling. Chromosome spreads were prepared as previously described and visualized under
518 the microscope to identify those slides with meiocytes at the desired stages. The slides were
519 incubated in a Coplin jar with 100% ethanol to detach the coverslip and washed with 1×PBST
520 (0.1% Triton X-100 in 1×PBS. Another glass staining jar was filled with tri-sodium citrate
521 buffer pH7 and heated to boiling point in a microwave. The slides were placed in the heated
522 tri-sodium citrate solution for 45 seconds, after which they were returned to room
523 temperature 1×PBST.

524 The rabbit anti-MLH1 primary antibodies (kindly provided by Mathilde Grelon, INRAe
525 Versailles [38]) was prepared at 1/200 in 1×PBST + 1% BSA. A 45µl drop was placed on a
526 32x24mm piece of parafilm and the inverted slide place on this. The slides were incubated for
527 2 days at 4°C in a dark moist chamber, after which they were washed 3 x 5 minutes with
528 1×PBST. The secondary antibodies (goat anti-rabbit Alexa fluor 488) was prepared at 1/100
529 1×in PBST + 1% BSA, and 45µl were used per slide. Slides were incubated 30 minutes at 37°C

530 in a dark moist chamber, after which they were washed 2 x 5 minutes in 1×PBST, followed by
531 one wash with 1×PBS. The Click-iT reaction was then performed as described above and the
532 slide was mounted in Vectashield + DAPI mounting medium for microscopy. Counting of
533 MLH1 foci and co-localization with EdU foci was carried out by visual inspection of images
534 taken using the Zeiss LSM800 confocal microscope plus the Airyscan module.

535

536

537

538 ## Acknowledgements

539 We thank the members of the recombination group and especially Olivier Da Ines,
540 Jérémy Verbeke and Floriane Chéron for their help and suggestions. Mathilde Grelon kindly
541 sent us the anti-MLH1 antiserum.

542 This work was supported by a European Marie Sklodowska Curie Actions Innovative
543 Training Network grant (EU H2020-MSCA-ITN-2017-765212) to CIW, the Centre National de
544 Recherche Scientifique (CNRS), the Institut National de la Santé et de la Recherche Médicale
545 (Inserm) and the Université Clermont Auvergne. The funders had no role in study design,
546 data collection and analysis, decision to publish, or preparation of the manuscript.

547

548

549

550 ## References

551 1. Arter M, Keeney S. Divergence and conservation of the meiotic recombination
552 machinery. Nat Rev Genet. 2023 [cited 6 Feb 2024]. doi:10.1038/s41576-023-00669-8

553 2. Hotta Y, Stern H. Transient phosphorylation of deoxyribosides and regulation of
554 deoxyribonucleic acid synthesis. J Biophys Biochem Cytol. 1961/11/01 ed. 1961;11:
555 311–9. doi:10.1083/jcb.11.2.311

556 3. Lima-De-Faria A, German J, Ghatnekar M, McGovern J, Anderson L. In vitro labelling of
557 human meiotic chromosomes with H3-thymidine. Hereditas. 1968;60: 249–261.
558 doi:10.1111/j.1601-5223.1968.tb02205.x

559 4. Mukherjee AB, Cohen MM. DNA Synthesis during Meiotic Prophase in Male Mice.
560 Nature. 1968;219: 489–490. doi:10.1038/219489a0

561 5. Prensky W. Uptake of thymine-methy6H3 by pachytene chromosomes of Lilium
562 longiflorum. Genetics. 1962;47: 977.

563 6. Wimber DE, Prensky W. Autoradiography with Meiotic Chromosomes of the Male Newt
564 (Triturus Viridescens) Using H3-Thymidine. Genetics. 1963/12/01 ed. 1963;48: 1731–8.
565 doi:10.1093/genetics/48.12.1731

566 7. Carpenter AT. EM autoradiographic evidence that DNA synthesis occurs at
567 recombination nodules during meiosis in Drosophila melanogaster females.
568 Chromosoma. 1981/01/01 ed. 1981;83: 59–80. doi:10.1007/BF00286016

569 8. Moses MJ, Dresser ME, Poorman PA. Composition and role of the synaptonemal

570 complex. Symp Soc Exp Biol. 1984/01/01 ed. 1984;38: 245–70.

571 9. Terasawa M, Ogawa H, Tsukamoto Y, Shinohara M, Shirahige K, Kleckner N, et al.
572 Meiotic recombination-related DNA synthesis and its implications for cross-over and
573 non-cross-over recombinant formation. Proc Natl Acad Sci U S A. 2007/03/27 ed.
574 2007;104: 5965–70. doi:10.1073/pnas.0611490104

575 10. Loidl J, Lukaszewicz A, Howard-Till RA, Koestler T. The Tetrahymena meiotic
576 chromosome bouquet is organized by centromeres and promotes interhomolog
577 recombination. J Cell Sci. 2012/09/15 ed. 2012;125: 5873–80. doi:10.1242/jcs.112664

578 11. Armstrong SJ, Franklin FCH, Jones GH. A meiotic time-course for Arabidopsis thaliana.
579 Sex Plant Reprod. 2003;16: 141–149. doi:10.1007/s00497-003-0186-4

580 12. Stronghill PE, Azimi W, Hasenkampf CA. A novel method to follow meiotic progression
581 in Arabidopsis using confocal microscopy and 5-ethynyl-2′-deoxyuridine labeling. Plant
582 Methods. 2014;10: 33. doi:10.1186/1746-4811-10-33

583 13. Sanchez-Moran E, Santos J-L, Jones GH, Franklin FCH. ASY1 mediates AtDMC1-
584 dependent interhomolog recombination during meiosis in Arabidopsis. Gene Dev.
585 2007;21: 2220–2233. doi:10.1101/gad.439007

586 14. Allers T, Lichten M. Differential Timing and Control of Noncrossover and Crossover
587 Recombination during Meiosis. Cell. 2001;106: 47–57. doi:10.1016/s0092-
588 8674(01)00416-0

589 15. Börner GV, Hochwagen A, MacQueen AJ. Meiosis in budding yeast. Rothstein R, editor.
590 GENETICS. 2023;225: iyad125. doi:10.1093/genetics/iyad125

591 16. Collins I, Newlon CS. Meiosis-specific formation of joint DNA molecules containing

592 sequences from homologous chromosomes. Cell. 1994;76: 65–75. doi:10.1016/0092-
593 8674(94)90173-2

594 17. Hunter N, Kleckner N. The Single-End Invasion: An Asymmetric Intermediate at the
595 Double-Strand Break to Double-Holliday Junction Transition of Meiotic Recombination.
596 Cell. 2001;106: 59–70. doi:10.1016/S0092-8674(01)00430-5

597 18. Schwacha A, Kleckner N. Identification of joint molecules that form frequently between
598 homologs but rarely between sister chromatids during yeast meiosis. Cell. 1994;76: 51–
599 63. doi:10.1016/0092-8674(94)90172-4

600 19. Wijnker E, James GV, Ding J, Becker F, Klasen JR, Rawat V, et al. The genomic landscape
601 of meiotic crossovers and gene conversions in Arabidopsis thaliana. eLife. 2013;2:
602 e01426. doi:10.7554/elife.01426

603 20. Lu P, Han X, Qi J, Yang J, Wijeratne AJ, Li T, et al. Analysis of Arabidopsis genome-wide
604 variations before and after meiosis and meiotic recombination by resequencing
605 Landsberg erecta and all four products of a single meiosis. 2012;22: 508–518.
606 doi:10.1101/gr.127522.111

607 21. Li R, Bitoun E, Altemose N, Davies RW, Davies B, Myers SR. A high-resolution map of
608 non-crossover events reveals impacts of genetic diversity on mammalian meiotic
609 recombination. Nat Commun. 2019;10: 3900. doi:10.1038/s41467-019-11675-y

610 22. Serrentino M-EM, Borde VV. The spatial regulation of meiotic recombination hotspots:
611 are all DSB hotspots crossover hotspots? Experimental cell research. 2012;318: 1347–
612 1352. doi:10.1016/j.yexcr.2012.03.025

613 23. Chakraborty P, Pankajam AV, Lin G, Dutta A, Krishnaprasad GN, Tekkedil MM, et al.

614 Modulating Crossover Frequency and Interference for Obligate Crossovers in
615 Saccharomyces cerevisiae Meiosis. G3 (Bethesda). 2017;7: 1511–1524.
616 doi:10.1534/g3.117.040071

617 24. Mancera E, Bourgon R, Brozzi A, Huber W, Steinmetz LM. High-resolution mapping of
618 meiotic crossovers and non-crossovers in yeast. Nature. 2008;454: 479–485.
619 doi:10.1038/nature07135

620 25. Valuchova S, Mikulkova P, Pecinkova J, Klimova J, Krumnikl M, Bainar P, et al. Imaging
621 plant germline differentiation within Arabidopsis flowers by light sheet microscopy.
622 eLife. 2020;9: 3645–19. doi:10.7554/elife.52546

623 26. Rossig C, Lievre LL, Pilkington SM, Brownfield L. A simple and rapid method for imaging
624 male meiotic cells in anthers of model and non-model plant species. Plant Reprod.
625 2021;34: 37–46. doi:10.1007/s00497-021-00404-5

626 27. Prusicki MA, Keizer EM, Rosmalen RP van, Komaki S, Seifert F, Müller K, et al. Live cell
627 imaging of meiosis in Arabidopsis thaliana. eLife. 2019;8: e42834.
628 doi:10.7554/elife.42834

629 28. Kurzbauer M-T, Uanschou C, Chen D, Schlögelhofer P. The recombinases DMC1 and
630 RAD51 are functionally and spatially separated during meiosis in Arabidopsis. Plant Cell.
631 2012;24: 2058–2070. doi:10.1105/tpc.112.098459

632 29. Singh G, Da Ines O, Gallego ME, White CI. Analysis of the impact of the absence of
633 RAD51 strand exchange activity in Arabidopsis meiosis. PLoS ONE. 2017;12: e0183006-
634 16. doi:10.1371/journal.pone.0183006

635 30. Varas J, Graumann K, Osman K, Pradillo M, Evans DE, Santos JL, et al. Absence of SUN1

636 and SUN2 proteins in Arabidopsis thaliana leads to a delay in meiotic progression and
637 defects in synapsis and recombination. Plant J. 2015;81: 329–346.
638 doi:10.1111/tpj.12730

639 31. Concia L, Brooks AM, Wheeler E, Zynda GJ, Wear EE, LeBlanc C, et al. Genome-Wide
640 Analysis of the Arabidopsis Replication Timing Program. PLANT PHYSIOLOGY. 2018;176:
641 2166–2185. doi:10.1104/pp.17.01537

642 32. Da Ines O, White CI. Centromere Associations in Meiotic Chromosome Pairing. Annual
643 review of genetics. 2015;49: 95–114. doi:10.1146/annurev-genet-112414-055107

644 33. Koornneef M, Fransz P, Jong H de. Cytogenetic tools for Arabidopsis thaliana.
645 Chromosom Res. 2003;11: 183–194. doi:10.1023/a:1022827624082

646 34. Naish M, Alonge M, Wlodzimierz P, Tock AJ, Abramson BW, Schmücker A, et al. The
647 genetic and epigenetic landscape of the Arabidopsis centromeres. Science. 2021;374:
648 eabi7489. doi:10.1126/science.abi7489

649 35. Rowan BA, Heavens D, Feuerborn TR, Tock AJ, Henderson IR, Weigel D. An Ultra High-
650 Density Arabidopsis thaliana Crossover Map That Refines the Influences of Structural
651 Variation and Epigenetic Features. Genetics. 2019;213: genetics.302406.2019.
652 doi:10.1534/genetics.119.302406

653 36. Choi K, Zhao X, Tock AJ, Lambing C, Underwood CJ, Hardcastle TJ, et al. Nucleosomes
654 and DNA methylation shape meiotic DSB frequency in Arabidopsis thaliana transposons
655 and gene regulatory regions. Genome research. 2018;28: 532–546.
656 doi:10.1101/gr.225599.117

657 37. Grelon M, Vezon D, Gendrot G, Pelletier G. AtSPO11-1 is necessary for efficient meiotic

658 recombination in plants. EMBO J. 2001;20: 589–600. doi:10.1093/emboj/20.3.589

659 38. Chelysheva L, Grandont L, Vrielynck N, le Guin S, Mercier R, Grelon M. An Easy Protocol
660 for Studying Chromatin and Recombination Protein Dynamics during
661 Arabidopsisthaliana Meiosis: Immunodetection of Cohesins, Histones and MLH1.
662 Cytogenetic and Genome Research. 2010;129: 143–153. doi:10.1159/000314096

663 39. Schwacha A, Kleckner N. Interhomolog Bias during Meiotic Recombination: Meiotic
664 Functions Promote a Highly Differentiated Interhomolog-Only Pathway. Cell. 1997;90:
665 1123–1135. doi:10.1016/S0092-8674(00)80378-5

666 40. Goldfarb T, Lichten M. Frequent and efficient use of the sister chromatid for DNA
667 double-strand break repair during budding yeast meiosis. PLoS biology. 2010;8:
668 e1000520. doi:10.1371/journal.pbio.1000520

669 41. Oh SD, Lao JP, Hwang PY-H, Taylor AF, Smith GR, Hunter N. BLM Ortholog, Sgs1,
670 Prevents Aberrant Crossing-over by Suppressing Formation of Multichromatid Joint
671 Molecules. Cell. 2007;130: 259–272. doi:10.1016/j.cell.2007.05.035

672 42. Oh SD, Lao JP, Taylor AF, Smith GR, Hunter N. RecQ Helicase, Sgs1, and XPF Family
673 Endonuclease, Mus81-Mms4, Resolve Aberrant Joint Molecules during Meiotic
674 Recombination. Molecular Cell. 2008;31: 324–336. doi:10.1016/j.molcel.2008.07.006

675 43. Jackson JA, Fink GR. Meiotic recombination between duplicated genetic elements in
676 Saccharomyces cerevisiae. Genetics. 1985;109: 303–332.
677 doi:10.1093/genetics/109.2.303

678 44. Haber JE, Thorburn PC, Rogers D. Meiotic and mitotic behaviour of dicentric
679 chromosomes in Saccharomyces cerevisiae. Genetics. 1984;106: 185–205.

680 doi:10.1093/genetics/106.2.185

681 45. Webber HA, Howard L, Bickel SE. The cohesion protein ORD is required for homologue
682 bias during meiotic recombination. The Journal of Cell Biology. 2004;164: 819–829.
683 doi:10.1083/jcb.200310077

684 46. Cole F, Baudat F, Grey C, Keeney S, De Massy B, Jasin M. Mouse tetrad analysis provides
685 insights into recombination mechanisms and hotspot evolutionary dynamics. Nat
686 Genet. 2014;46: 1072–1080. doi:10.1038/ng.3068

687 47. Almanzar DE, Gordon SG, Rog O. Meiotic sister chromatid exchanges are rare in C.
688 elegans. Current Biology. 2021;31: 1499-1507.e3. doi:10.1016/j.cub.2020.11.018

689 48. Toraason E, Horacek A, Clark C, Glover ML, Adler VL, Premkumar T, et al. Meiotic DNA
690 break repair can utilize homolog-independent chromatid templates in C. elegans.
691 Current Biology. 2021;31: 1508-1514.e5. doi:10.1016/j.cub.2021.03.008

692 49. Billmyre KK, Hughes SE. Meiosis: The elusive sister chromatid repair. Current Biology.
693 2021;31: R454–R456. doi:10.1016/j.cub.2021.03.093

694 50. Yang S, Yuan Y, Wang L, Li J, Wang W, Liu H, et al. Great majority of recombination
695 events in Arabidopsis are gene conversion events. Proceedings of the National
696 Academy of Sciences of the United States of America. 2012;109: 20992–20997.
697 doi:10.1073/pnas.1211827110

698 51. Drouaud J, Khademian H, Giraut L, Zanni V, Bellalou S, Henderson IR, et al. Contrasted
699 patterns of crossover and non-crossover at Arabidopsis thaliana meiotic recombination
700 hotspots. Hong Ma, editor. PLoS Genetics. 2013;9: e1003922.
701 doi:10.1371/journal.pgen.1003922

702 52. Sims J, Schlögelhofer P, Kurzbauer M-T. From Microscopy to Nanoscopy: Defining an
703 Arabidopsis thaliana Meiotic Atlas at the Nanometer Scale. Front Plant Sci. 2021;12:
704 672914. doi:10.3389/fpls.2021.672914

705 53. Fayos I, Meunier AC, Vernet A, Navarro-Sanz S, Portefaix M, Lartaud M, et al.
706 Assessment of the roles of SPO11-2 and SPO11-4 in meiosis in rice using CRISPR/Cas9
707 mutagenesis. Journal of Experimental Botany. 2020;71: 7046–7058.
708 doi:10.1093/jxb/eraa391

709 54. Stacey NJ, Kuromori T, Azumi Y, Roberts G, Breuer C, Wada T, et al. Arabidopsis SPO11-
710 2 functions with SPO11-1 in meiotic recombination. The Plant Journal. 2006;48: 206–
711 216. doi:10.1111/j.1365-313X.2006.02867.x

712 55. Sims J, Copenhaver GP, Schlögelhofer P. Meiotic DNA Repair in the Nucleolus Employs a
713 Nonhomologous End-Joining Mechanism. The Plant Cell. 2019;31: 2259–2275.
714 doi:10.1105/tpc.19.00367

715 56. Vrielynck N, Schneider K, Rodriguez M, Sims J, Chambon A, Hurel A, et al. Conservation
716 and divergence of meiotic DNA double strand break forming mechanisms in
717 Arabidopsis thaliana. Nucleic Acids Res. 2021. doi:10.1093/nar/gkab715

718 57. Sprink T, Hartung F. Heterologous Complementation of SPO11-1 and -2 Depends on the
719 Splicing Pattern. IJMS. 2021;22: 9346. doi:10.3390/ijms22179346

720 58. Vrielynck N, Chambon A, Vezon D, Pereira L, Chelysheva L, Muyt AD, et al. A DNA
721 topoisomerase VI–like complex initiates meiotic recombination. Science (New York,
722 NY). 2016;351: 939–943. doi:10.1126/science.aad5196

723 59. Hartung F, Wurz-Wildersinn R, Fuchs J, Schubert I, Suer S, Puchta H. The catalytically

active tyrosine residues of both SPO11-1 and SPO11-2 are required for meiotic double-strand break induction in Arabidopsis. The Plant cell. 2007;19: 3090–3099. doi:10.1105/tpc.107.054817

60. Alonso-Ramos P, Álvarez-Melo D, Strouhalova K, Pascual-Silva C, Garside GB, Arter M, et al. The Cdc14 Phosphatase Controls Resolution of Recombination Intermediates and Crossover Formation during Meiosis. Int J Mol Sci. 2021;22: 9811. doi:10.3390/ijms22189811

61. Schubert I, Schubert V, Fuchs J. No Evidence for “Break-Induced Replication” in a Higher Plant – But Break-Induced Conversion May Occur. Front Plant Sci. 2011;2: 8. doi:10.3389/fpls.2011.00008

62. Vannier J-B, Depeiges A, White C, Gallego ME. Two roles for Rad50 in telomere maintenance. The EMBO Journal. 2006;25: 4577–4585. doi:10.1038/sj.emboj.7601345

63. Ross KJ, Fransz P, Jones GH. A light microscopic atlas of meiosis in Arabidopsis thaliana. Chromosom Res : Int J Mol, Supramol Evol Asp Chromosom Biol. 1996;4: 507–16. doi:10.1007/bf02261778

64. Dvořáčková M, Raposo B, Matula P, Fuchs J, Schubert V, Peška V, et al. Replication of ribosomal DNA in Arabidopsis occurs both inside and outside the nucleolus during S phase progression. J Cell Sci. 2017;131: jcs202416. doi:10.1242/jcs.202416

65. Lambing C, Osman K, Nuntasoontorn K, West A, Higgins JD, Copenhaver GP, et al. Arabidopsis PCH2 Mediates Meiotic Chromosome Remodeling and Maturation of Crossovers. PLoS Genet. 2015;11: e1005372. doi:10.1371/journal.pgen.1005372

66. Vanstraelen M, Baloban M, Ines OD, Cultrone A, Lammens T, Boudolf V, et al. APC/C-

746 CCS52A complexes control meristem maintenance in the Arabidopsis root. Proceedings
747 of the National Academy of Sciences of the United States of America. 2009;106:
748 11806–11811. doi:10.1073/pnas.0901193106

749 67. Amiard S, Charbonnel C, Allain E, Depeiges A, White CI, Gallego ME. Distinct roles of the
750 ATR kinase and the Mre11-Rad50-Nbs1 complex in the maintenance of chromosomal
751 stability in Arabidopsis. THE PLANT CELL. 2010;22: 3020–3033.
752 doi:10.1105/tpc.110.078527

753 68. Weisshart K, Fuchs J, Schubert V. Structured Illumination Microscopy (SIM) and
754 Photoactivated Localization Microscopy (PALM) to Analyze the Abundance and
755 Distribution of RNA Polymerase II Molecules on Flow-sorted Arabidopsis Nuclei. BIO-
756 PROTOCOL. 2016;6. doi:10.21769/BioProtoc.1725

757 69. Chelysheva LA, Grandont L, Grelon M. Immunolocalization of Meiotic Proteins in
758 Brassicaceae: Method 1. In: Pawlowski WP, Grelon M, Armstrong S, editors. Plant
759 Meiosis: Methods and Protocols. Totowa, NJ: Humana Press; 2013. pp. 93–101.
760 doi:10.1007/978-1-62703-333-6_9

761

762

763 ## Figure Legends

764 **Figure 1. EdU labelling strategy and timeline of** Arabidopsis **male meiosis.** Pollen mother cell nuclei
765 were fixed and isolated at the end of a 24-hour pulse of EdU incorporporation. Cells which traversed
766 all or part of the pre-meiotic S-phase during the pulse will show replicative EdU incorporation and be
767 at G2/leptotene/zygotene stages at the end of the pulse, with some overlap into early pachytene.
768 Fully pachytene nuclei (mid-late pachytene) will not show replicative labeling, but will have traversed
769 the leptotene and zygotene stages in the presence of EdU. Any EdU incorporation in these (or later)
770 nuclei will be due to non-S-Phase DNA synthesis.
771
772 **Figure 2. DSB repair-associated DNA synthesis tracts are detected from pachytene up to the end**
773 **of meiosis.** a) Meiosis I and b) meiosis II stages in *A. thaliana* wildtype. S-phase, replicative DNA
774 labelling is seen at early G2/letotene and zygotene stages, while clear, discrete foci of EdU substituted
775 DNA are visible in the chromosomes at later stages from pachytene onwards. Rectangles indicate the
776 enlarged regions presented in the zooms. Non-chromosomal EdU foci correspond to labelling of
777 mitochondrial genome replication. 3µm scale bars are shown at the bottom left of each image (1µm
778 for the zooms). Images were taken with the confocal microscope + Airyscan module.
779
780 **Figure 3. DSB repair-associated DNA synthesis is SPO11- dependent.**
781 a) Meiosis I and b) meiosis II stages in *A. thaliana* spo11-1 mutants. As for WT meiosis (Figure 2),
782 replicative S-phase labelling is seen at early stages, corresponding to G2/leptotene and zygotene. As
783 expected, a striking reduction in numbers of EdU foci (compared to WT) is observed in spo11-1
784 mutants at stages from mid-prophase I onwards (corresponding to pachytene and later
785 stages). Rectangles indicate the enlarged regions presented in the zooms. Images taken with the
786 confocal microscope with Airyscan module. 3µm scale bars are shown at the bottom left of each
787 image (1µm for the zooms).

788 **Figure 4. Concordance of numbers of SPO11-dependent, meiotic DNA synthesis foci and**
789 **estimated DSB numbers.**
790 a) Representative images of wild-type pachytene and *spo11-1* pachytene-like meiotic stages. The
791 merged DAPI (blue) plus EdU (orange) images are accompanied by the computer-generated images of
792 the scored EdU foci (white, right panels). EdU foci colocalising with chromosome fibres were retained
793 for counting and mean intensity used to exclude the much-brighter organellar foci (see text). The
794 Images taken with the confocal microscope with Airyscan module. 3µm scale bars are shown at the
795 bottom left of each image. b) Numbers of EdU foci on the chromosomes quantified with Imaris
796 software show clearly the SPO11-dependence of these DNA synthesis tracts and that their numbers
797 correspond to expectations from DSB counting in PMC. The mean number of foci/nucleus and
798 number of nuclei counted are shown above the graph.
799
800 **Figure 5. Ultrastructure of SPO11-dependent, meiotic DNA synthesis foci on the synaptonemal**
801 **complex (SC) during pachytene.**
802 a) Expected configurations of DNA synthesis tracts resulting from different mechanisms of
803 homologous recombinational repair of meiotic DSB: Synthesis-Dependent Strand Annealing (SDSA),
804 double-Holliday Junction (dHJ), Gene Conversion ± Crossover (GC±CO) and Break-Induced Replication
805 (BIR). b) Examples of segments of pachytene SC. Isolated individual foci (one SC lateral axis, white
806 circle) and pairs of foci on one homologue (one SC lateral axis, green circle) or the two homologues
807 (both SC lateral axes, yellow circle) are highlighted. The images represent a single slice of 3D-SIM
808 image stacks. 0.5µm scale bars are shown at the bottom left of each image.
809 **Figure 6. Class I crossovers (CO) colocalize with prophase I DNA synthesis tracts**.
810 a) Wild-type pachytene cell showing DAPI staining (blue), prophase I DNA synthesis tracts (EdU,
811 orange) and Class 1 CO (MLH1, green). **b)** Examples of colocalising and adjacent MLH1 and EdU foci.
812 The quantification (right) shows that 95.6% of MLH1 foci co-localize with EdU tracts, and the

813 remainder are adjacent to one. a) is a confocal image and b) a single slice of a 3D-SIM image stack.
814 Scale bars are 1µm in (a) and 0.1µm in (b).
815
816 **Figure 7. Recombination mechanisms and DNA synthesis tracts.**
817 Following resection and invasion of the donor chromatid (a), DNA neo-synthesis tracts resulting from
818 repair of DSB are expected to be found only on the recipient chromatid in gene conversions (f)
819 resulting from SDSA (b) or dHJ dissolution (e) pathways. A special case of this is the BIR pathway (c),
820 which will result in a long synthesis tract, potentially extending all the way to the end of the recipient
821 chromatid. DNA synthesis tracts are expected to be found on both the recipient and donor
822 chromatids in gene conversions, associated (g) or not (h) to a CO, resulting from resolution of the dHJ
823 intermediate (d).
824
825

826 Supplemental Figure Legends

827
828 **Figure S1. Discrete foci of EdU substituted DNA are visible in pachytene chromosomes of**
829 **Arabidopsis PMC.**
830 Examples of prophase I DNA labelling in pachtene nuclei of wildtype PMC. Each row is the same
831 nucleus, imaged with DAPI fluorescence (white, left), EdU (orange, middle) and the merged image
832 (right). Images taken with the confocal microscope with Airyscan module. 2µm scale bars are included
833 at the bottom left of each image.
834
835 **Figure S2. Distribution of SPO11-dependent, meiotic DNA synthesis foci on paired pachytene**
836 **chromosomes from two different cells.**

837 Zoomed regions from SIM (a) and Confocal (b) images of meiotic pachytenes, showing the distribution
838 of EdU-labelled meiotic prophase I DNA synthesis foci (a)red, b) orange) on the DAPI-stained
839 chromosome fibres (white) of the synaptonemal complexes. 0.5µm scale bars are included at the
840 bottom left of each image.

Figure 1

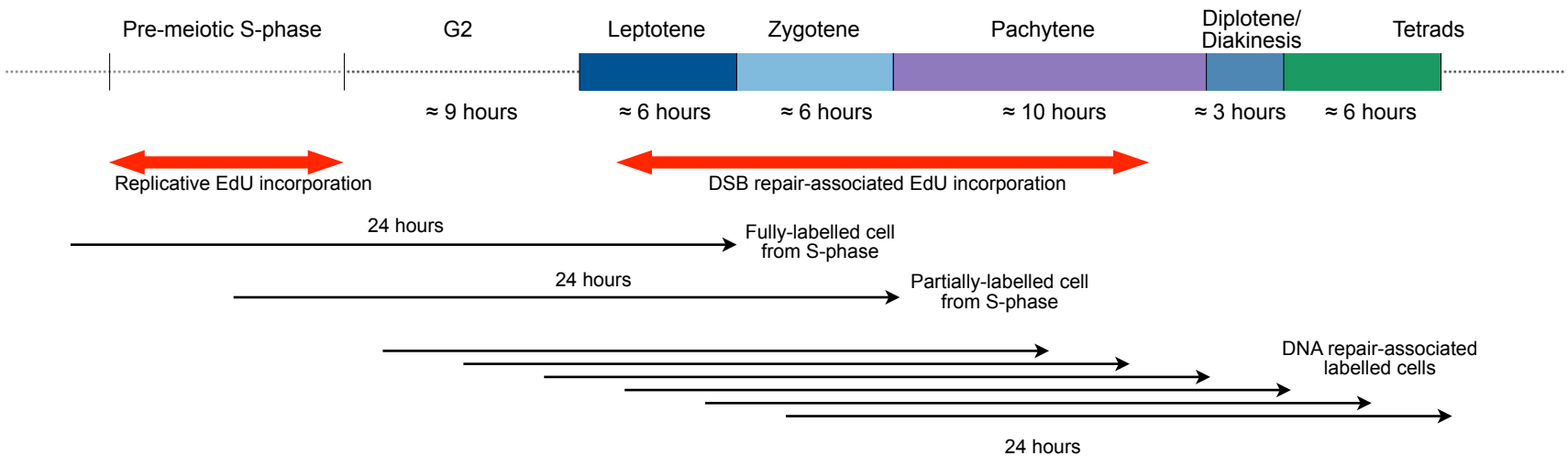

Figure 1. EdU labelling strategy and timeline of *Arabidopsis* male meiosis. Pollen mother cell nuclei were fixed and isolated at the end of a 24-hour pulse of EdU incorporporation. Cells which traversed all or part of the pre-meiotic S-phase during the pulse will show replicative EdU incorporation and be at G2/leptotene/zygotene stages at the end of the pulse, with some overlap into early pachytene. Fully pachytene nuclei (mid-late pachytene) will not show replicative labeling, but will have traversed the leptotene and zygotene stages in the presence of EdU. Any EdU incorporation in these (or later) nuclei will be due to non-S-Phase DNA synthesis.

Figure 2

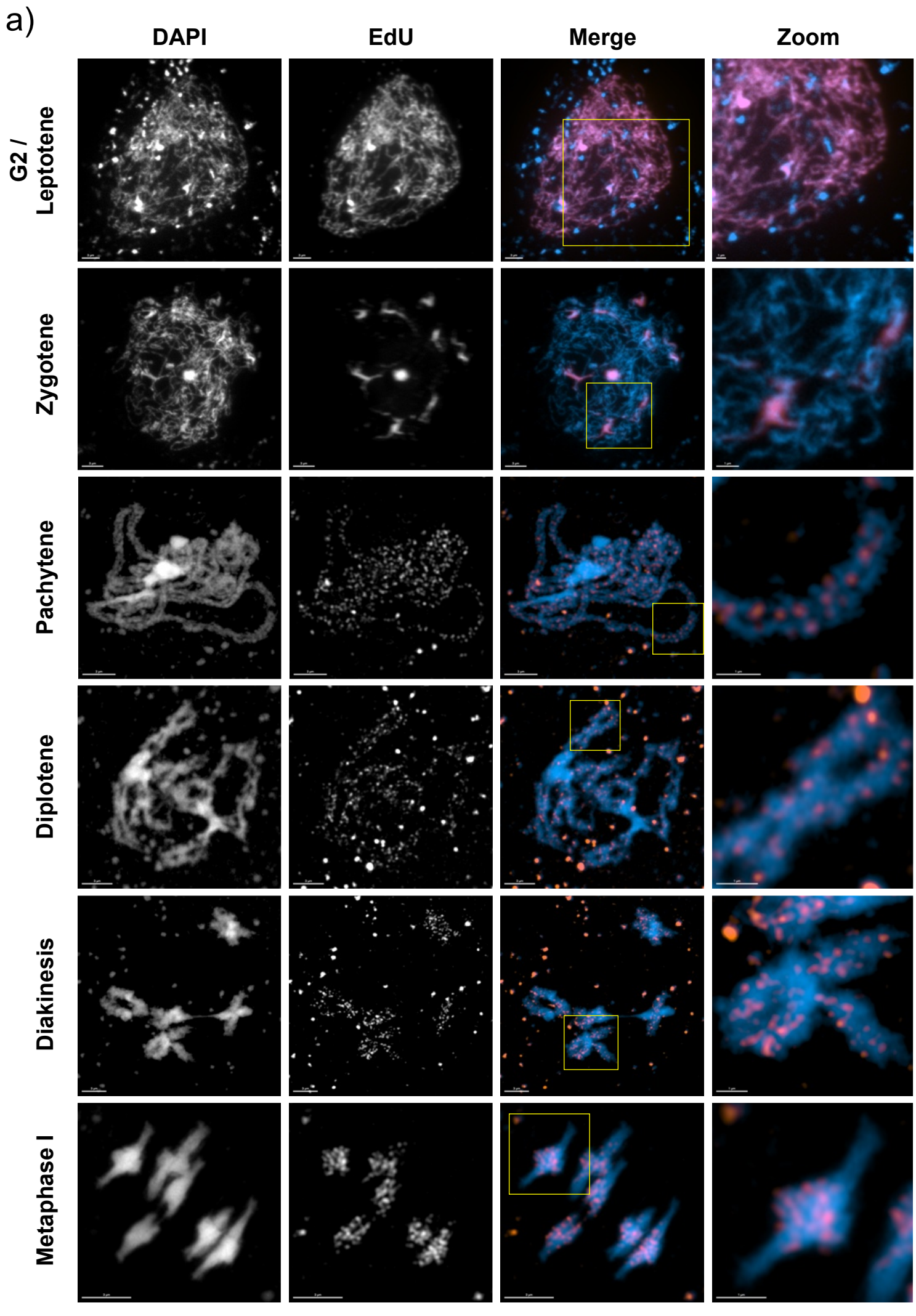
a)
DAPI
EdU
Merge
Zoom
G2 / Leptotene
Zygotene
Pachytene
Diplotene
Diakinesis
Metaphase I

Figure 2

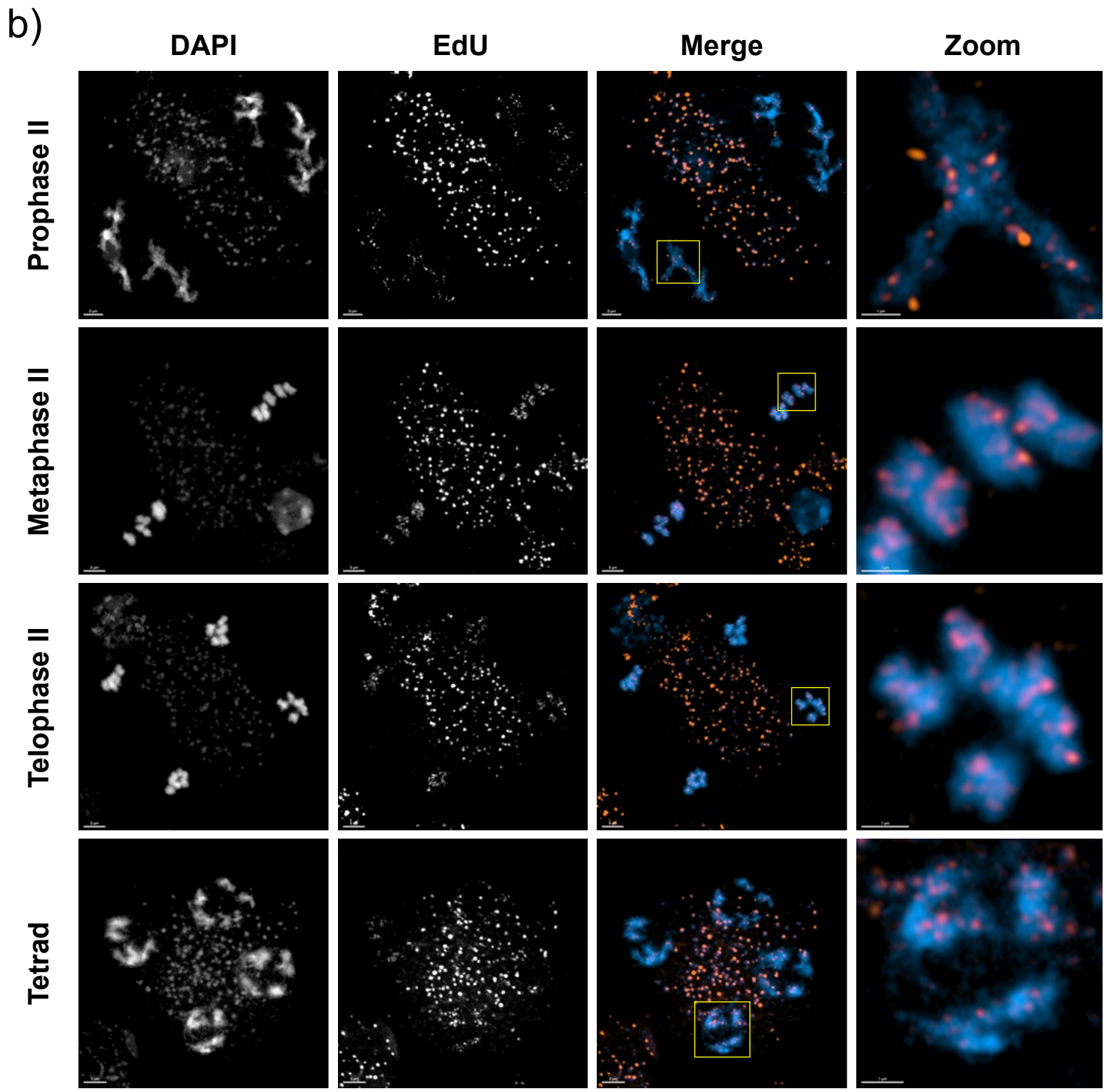

Figure 2. DSB repair-associated DNA synthesis tracts are detected from pachytene up to the end of meiosis.
a) Meiosis I and b) meiosis II stages in *A. thaliana* wildtype. S-phase, replicative DNA labelling is seen at early G2/letotene and zygotene stages, while clear, discrete foci of EdU substituted DNA are visible in the chromosomes at later stages from pachytene onwards. Rectangles indicate the enlarged regions presented in the zooms. Non-chromosomal EdU foci correspond to labelling of mitochondrial genome replication. 3µm scale bars are shown at the bottom left of each image (1µm for the zooms). Images were taken with the confocal microscope + Airyscan module.

Figure 3

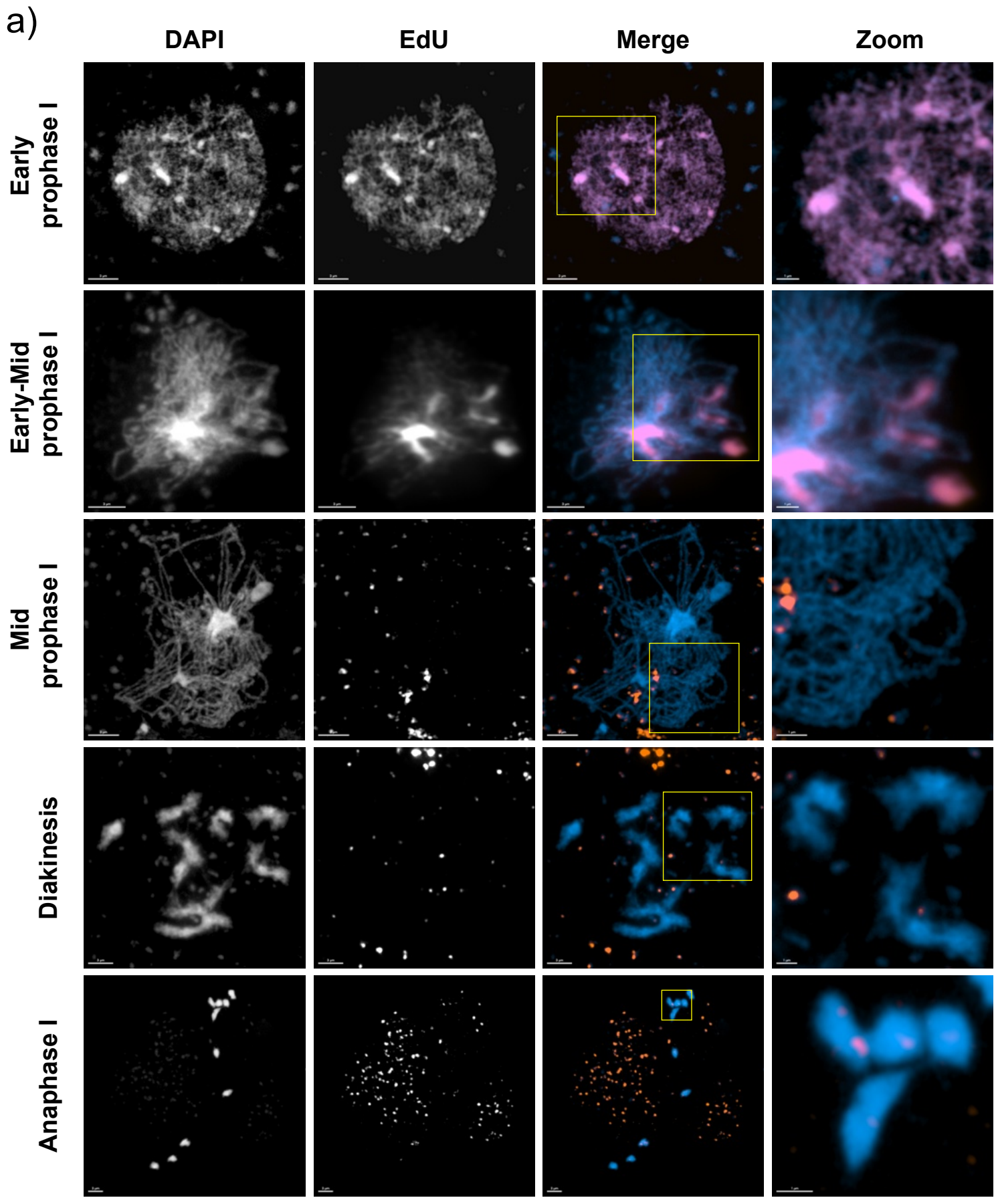
a)
DAPI
EdU
Merge
Zoom
Early prophase I
Early-Mid prophase I
Mid prophase I
Diakinesis
Anaphase I

Figure 3

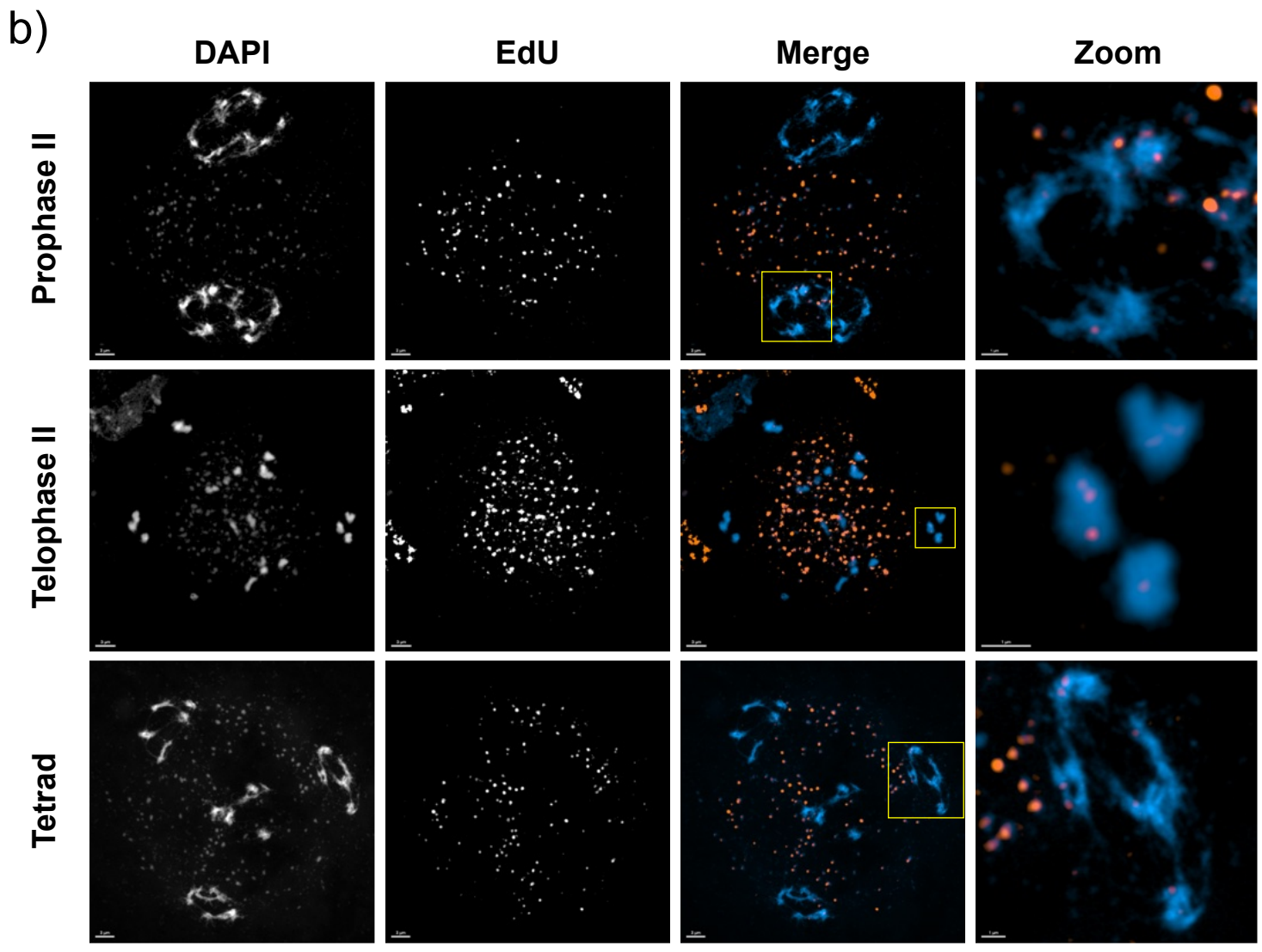

Figure 3. DSB repair-associated DNA synthesis is SPO11-dependent.
a) Meiosis I and b) meiosis II stages in *A. thaliana* spo11-1 mutants. As for WT meiosis (Figure 2), replicative S-phase labelling is seen at early stages, corresponding to G2/leptotene and zygotene. As expected, a striking reduction in numbers of EdU foci (compared to WT) is observed in spo11-1 mutants at stages from mid-prophase I onwards (corresponding to pachytene and later stages). Rectangles indicate the enlarged regions presented in the zooms. Images taken with the confocal microscope with Airyscan module. 3µm scale bars are shown at the bottom left of each image (1µm for the zooms).

Figure 4

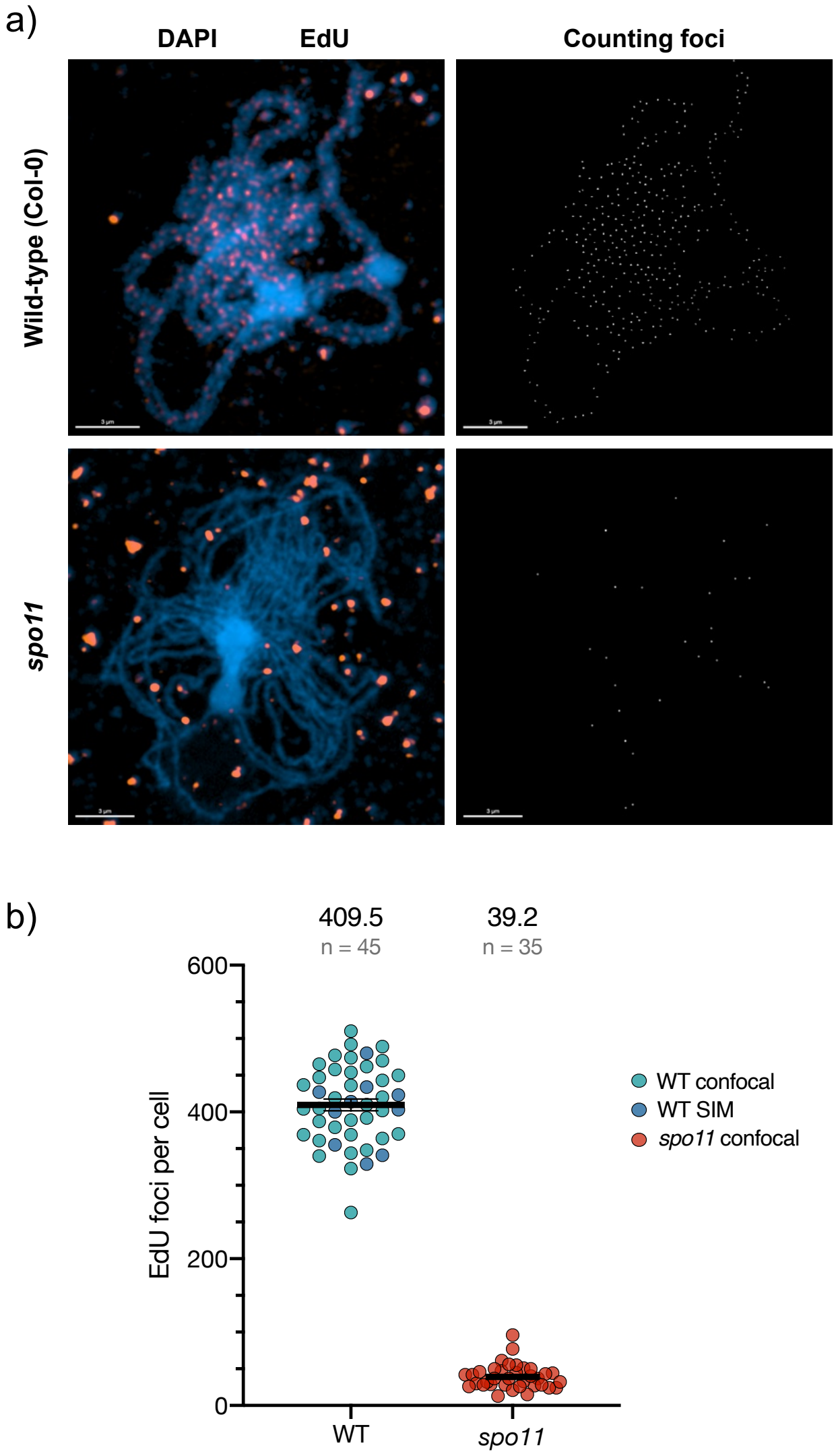

Figure 4. Concordance of numbers of SPO11-dependent, meiotic DNA synthesis foci and estimated DSB numbers. a) Representative images of wild-type pachytene and spo11-1 pachytene-like meiotic stages. The merged DAPI (blue) plus EdU (orange) images are accompanied by the computer-generated images of the scored EdU foci (white, right panels). EdU foci colocalising with chromosome fibres were retained for counting and mean intensity used to exclude the much-brighter organellar foci (see text). The Images taken with the confocal microscope with Airyscan module. 3μm scale bars are shown at the bottom left of each image. b) Numbers of EdU foci on the chromosomes quantified with Imaris software show clearly the SPO11-dependence of these DNA synthesis tracts and that their numbers correspond to expectations from DSB counting in PMC. The mean number of foci/nucleus and number of nuclei counted are shown above the graph.

Figure 5

a)

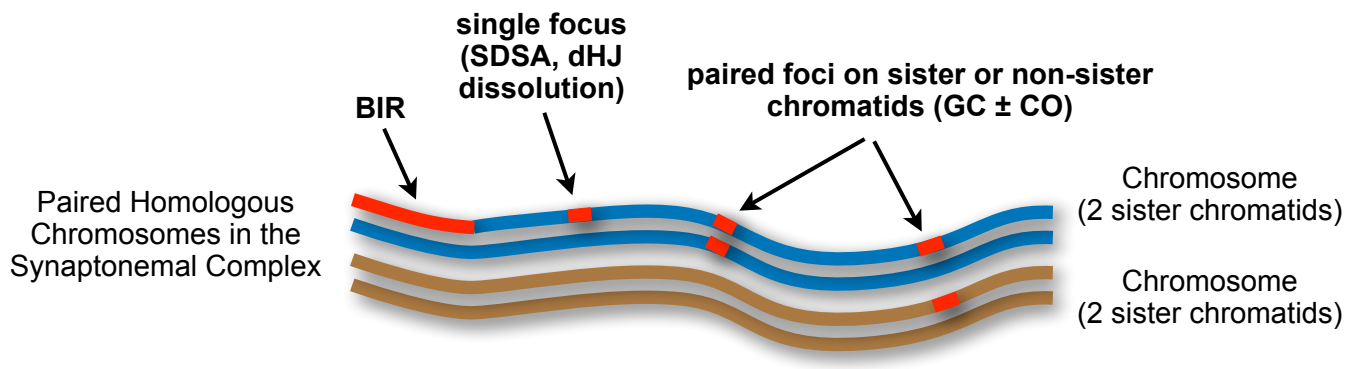

b)

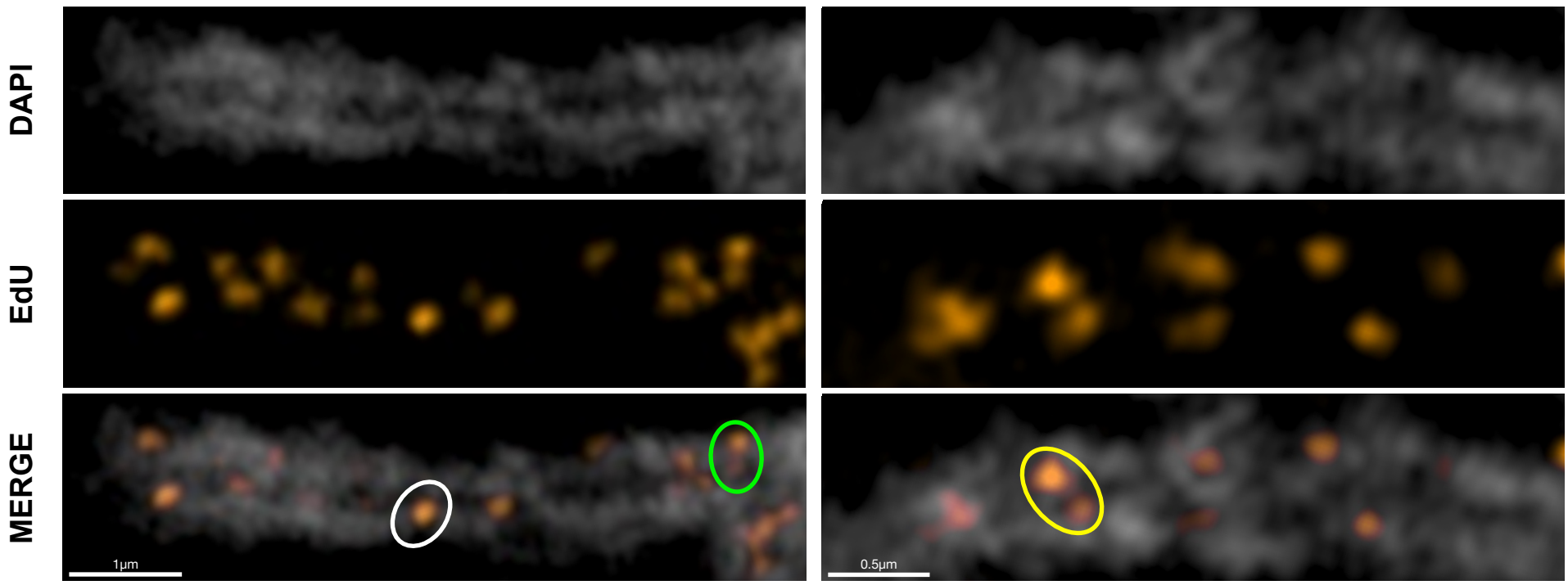

Figure 5. Ultrastructure of SPO11-dependent, meiotic DNA synthesis foci on the synaptonemal complex (SC) during pachytene. a) Expected configurations of DNA synthesis tracts resulting from different mechanisms of homologous recombinational repair of meiotic DSB: Synthesis-Dependent Strand Annealing (SDSA), double-Holliday Junction (dHJ), Gene Conversion ± Crossover (GC±CO) and Break-Induced Replication (BIR). b) Examples of segments of pachytene SC. Isolated individual foci (one SC lateral axis, white circle) and pairs of foci on one homologue (one SC lateral axis, green circle) or the two homologues (both SC lateral axes, yellow circle) are highlighted. The images represent a single slice of 3D-SIM image stacks. 0.5µm scale bars are shown at the bottom left of each image.

Figure 6

a)

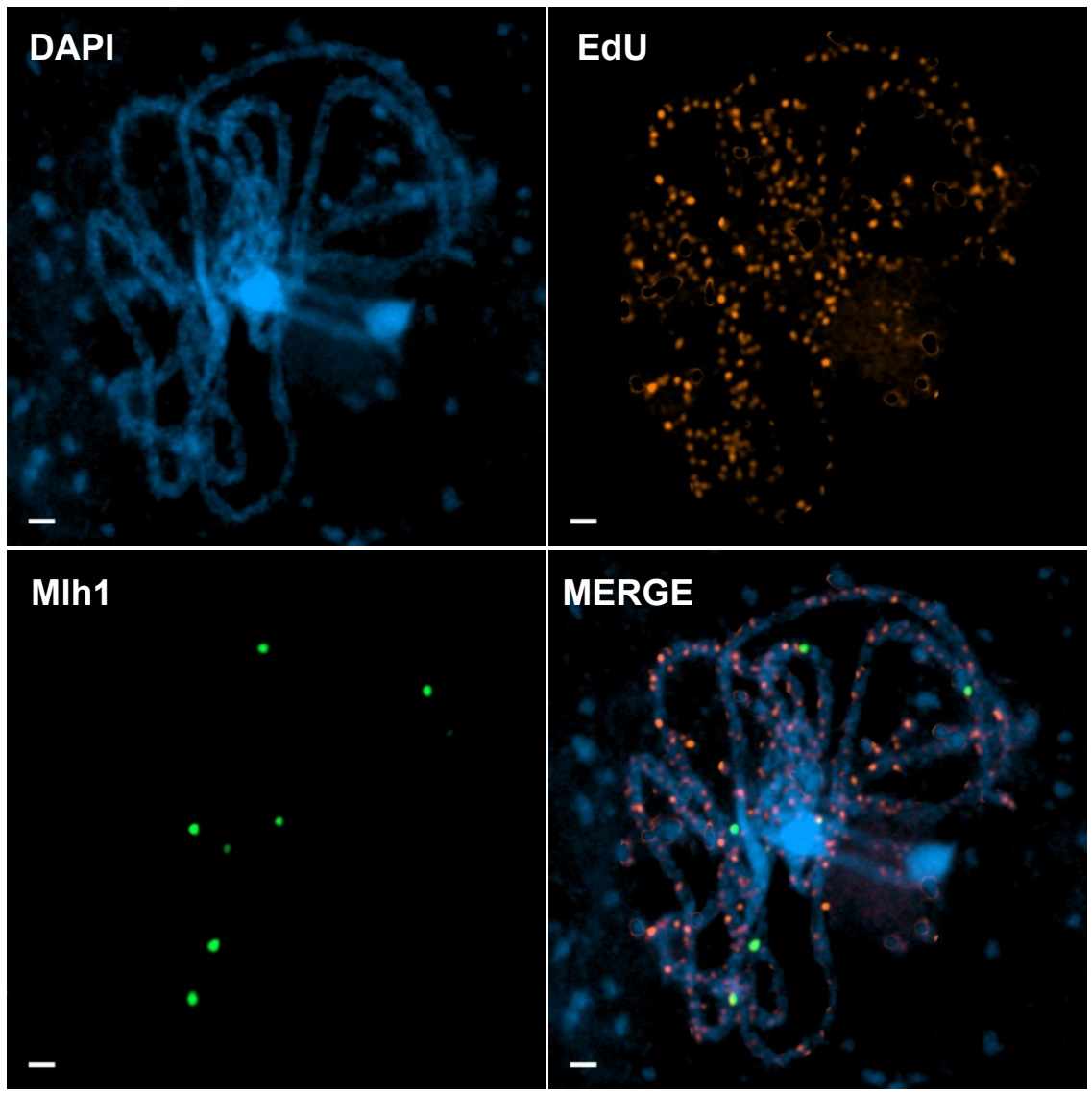

b)

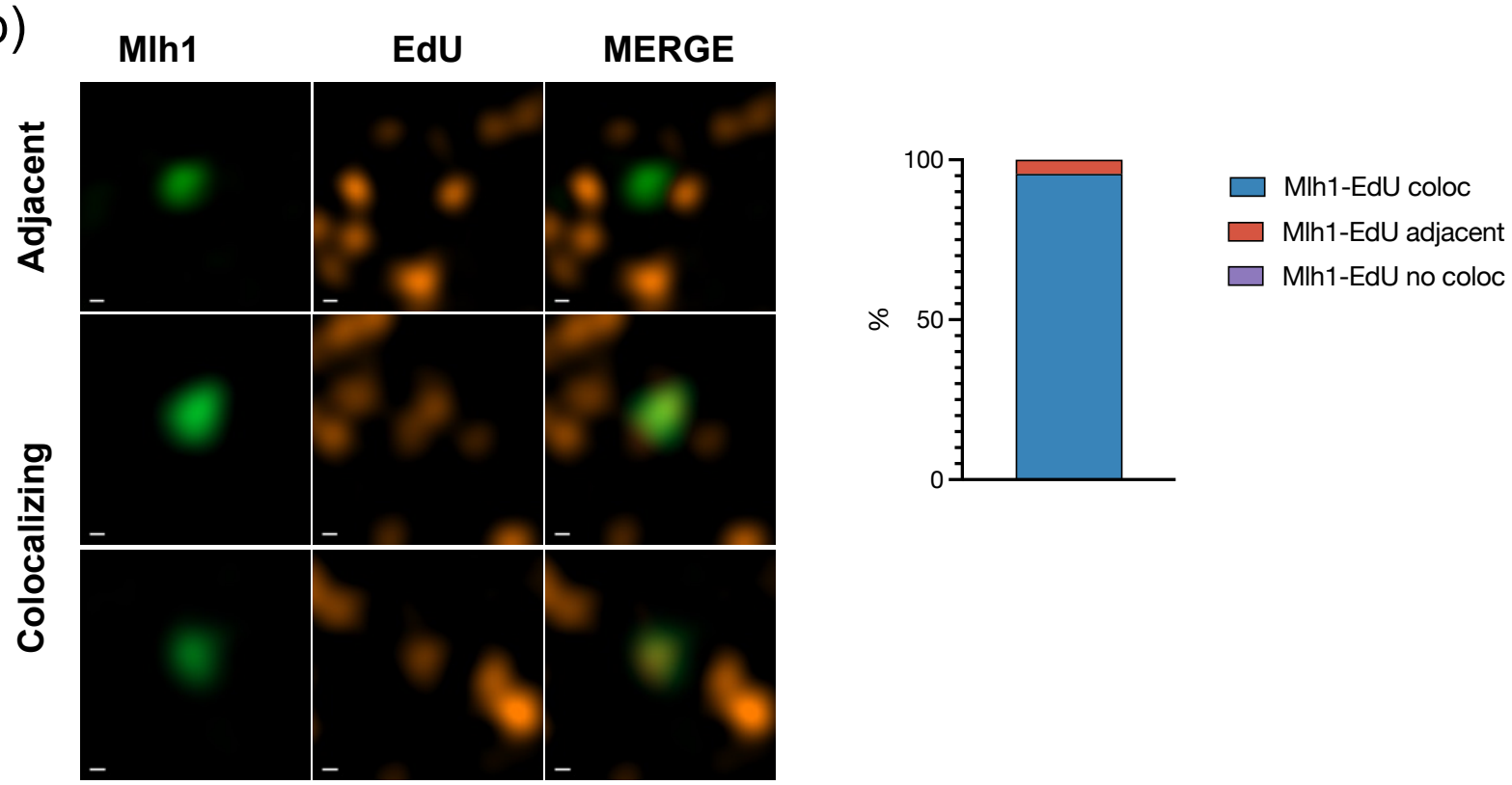

Figure 6. Class I crossovers (CO) colocalize with prophase I DNA synthesis tracts.
a) Wild-type pachytene cell showing DAPI staining (blue), prophase I DNA synthesis tracts (EdU, orange) and Class 1 CO (MLH1, green). b) Examples of colocalising and adjacent MLH1 and EdU foci. The quantification (right) shows that 95.6% of MLH1 foci co-localize with EdU tracts, and the remainder are adjacent to one. a) is a confocal image and b) a single slice of a 3D-SIM image stack. Scale bars are 1μm in (a) and 0.1μm in (b).

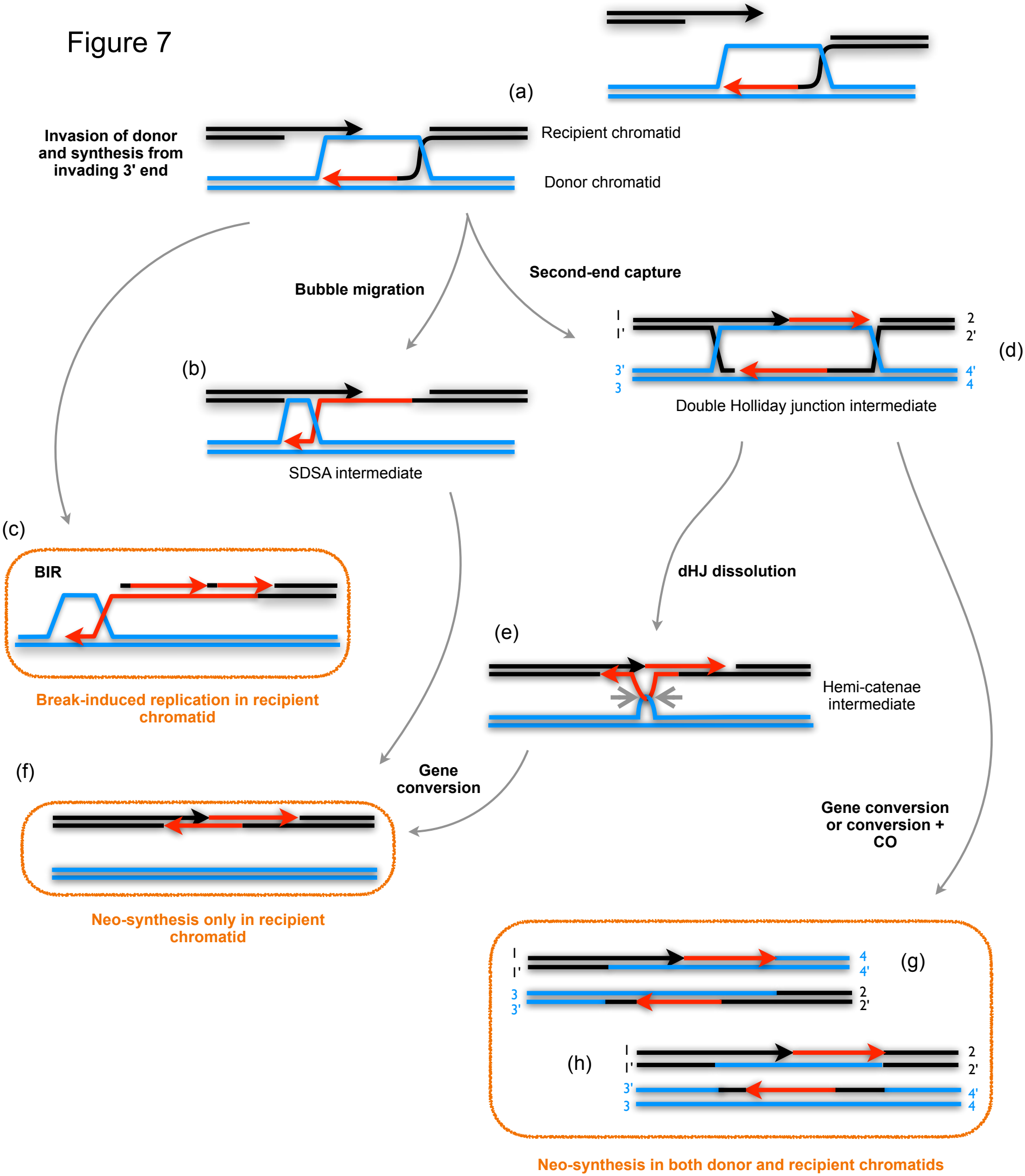

Figure 7. Recombination mechanisms and DNA synthesis tracts.
Following resection and invasion of the donor chromatid (a), DNA neo-synthesis tracts resulting from repair of DSB are expected to be found only on the recipient chromatid in gene conversions (f) resulting from SDSA (b) or dHJ dissolution (e) pathways. A special case of this is the BIR pathway (c), which will result in a long synthesis tract, potentially extending all the way to the end of the recipient chromatid. DNA synthesis tracts are expected to be found on both the recipient and donor chromatids in gene conversions, associated (g) or not (h) to a CO, resulting from resolution of the dHJ intermediate (d).

Supplemental Figure S1

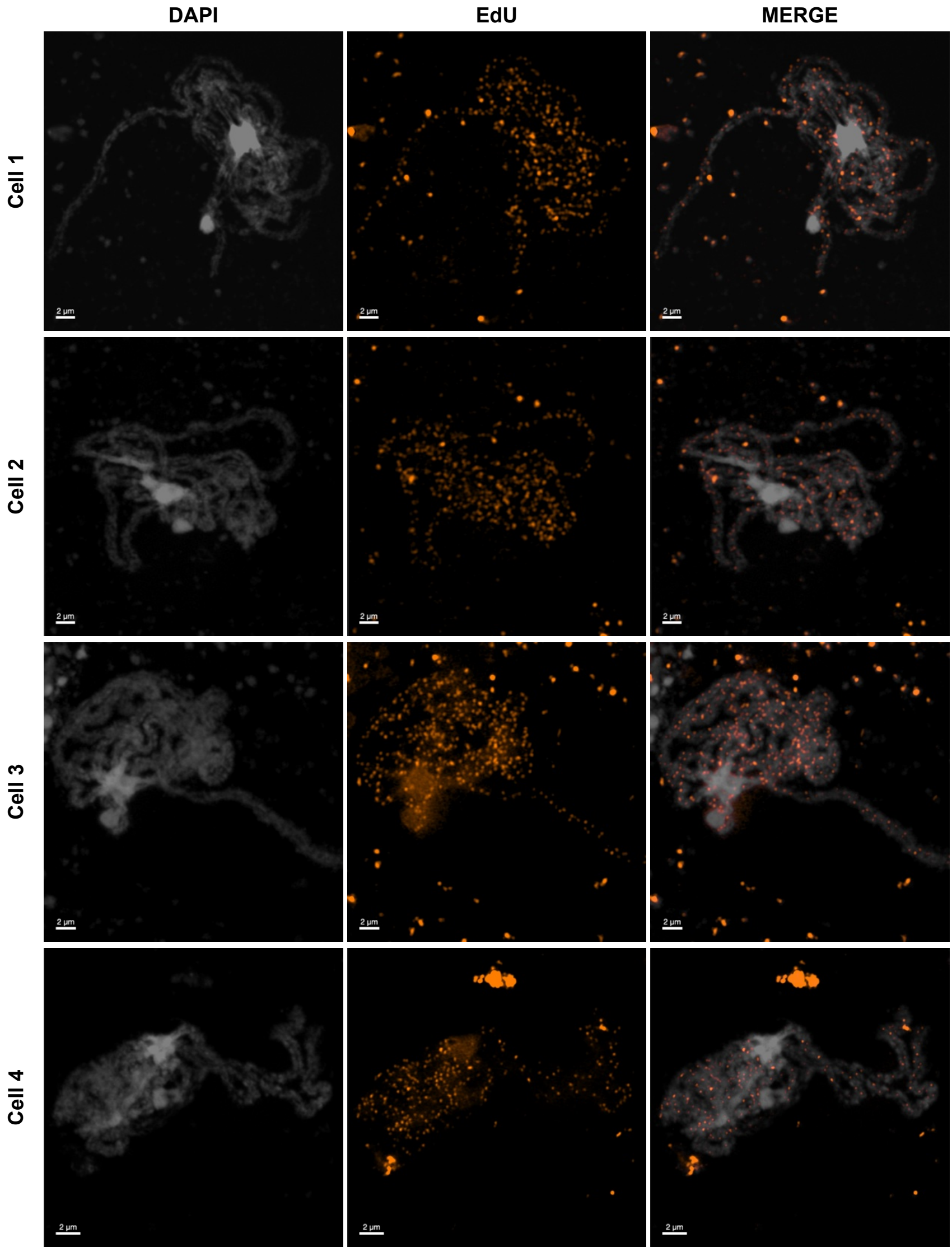

Supplemental Figure S1. Discrete foci of EdU substituted DNA are visible in pachytene chromosomes of Arabidopsis PMC.
Examples of prophase I DNA labelling in pachtene nuclei of wildtype PMC. Each row is the same nucleus, imaged with DAPI fluorescence (white, left), EdU (orange, middle) and the merged image (right). Images taken with the confocal microscope with Airyscan module. 2μm scale bars are included at the bottom left of each image.

Supplemental Figure S2

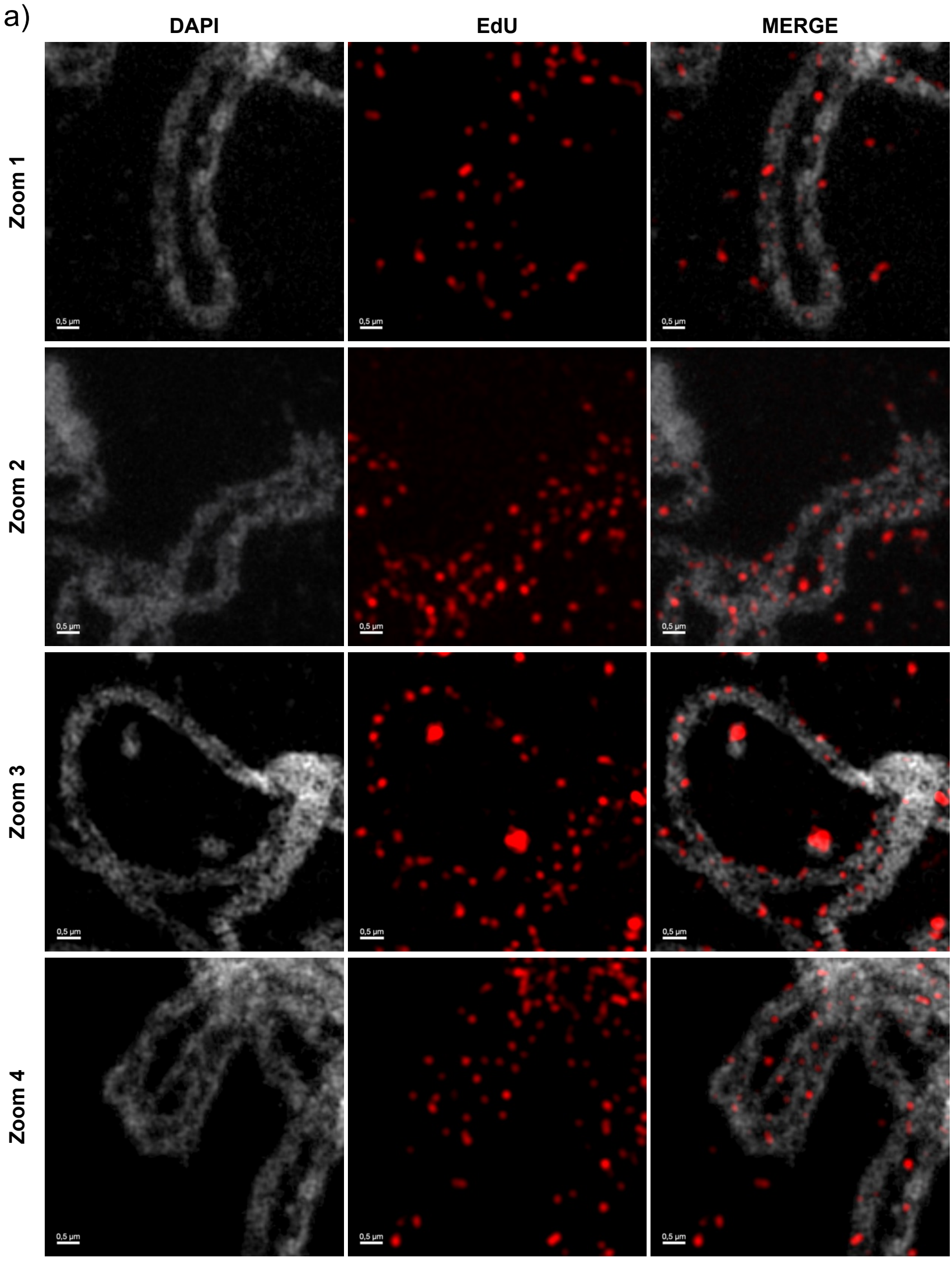

Supplemental Figure S2

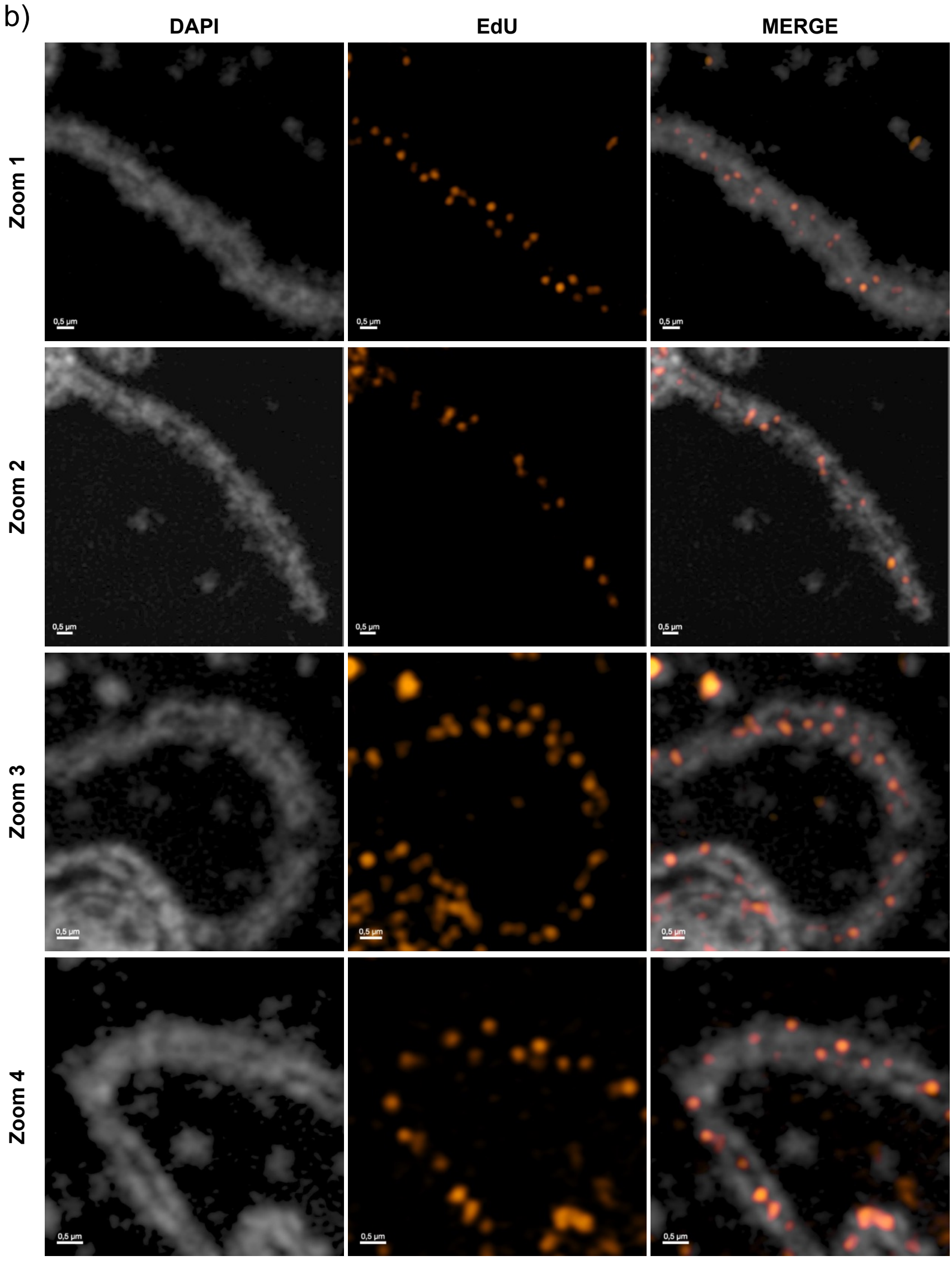

Supplemental Figure S2. Distribution of SPO11-dependent, meiotic DNA synthesis foci on paired pachytene chromosomes from two different cells.
Zoomed regions from SIM (a) and Confocal (b) images of meiotic pachytenes, showing the distribution of EdU-labelled meiotic prophase I DNA synthesis foci (a)red, b) orange) on the DAPI-stained chromosome fibres (white) of the synaptonemal complexes. 0.5μm scale bars are included at the bottom left of each image.